NASA TECHNICAL NOTE

NASA TN D-4238

NASA TN D-4238

TRANSIENT CHILLDOWN OF A SINGLE THICK-WALLED TUBE BY LIQUID AND GASEOUS HYDROGEN

by Francis C. Chenoweth, James J. Watt, and Earl L. Sprague

Lewis Research Center
Cleveland, Ohio

NATIONAL AERONAUTICS AND SPACE ADMINISTRATION • WASHINGTON, D. C. • NOVEMBER 1967

TRANSIENT CHILLDOWN OF A SINGLE THICK-WALLED TUBE BY LIQUID AND GASEOUS HYDROGEN

By Francis C. Chenoweth, James J. Watt, and Earl L. Sprague

Lewis Research Center
Cleveland, Ohio

NATIONAL AERONAUTICS AND SPACE ADMINISTRATION

For sale by the Clearinghouse for Federal Scientific and Technical Information
Springfield, Virginia 22151 – CFSTI price $3.00

TRANSIENT CHILLDOWN OF A SINGLE THICK-WALLED TUBE BY LIQUID AND GASEOUS HYDROGEN

by Francis C. Chenoweth, James J. Watt, and Earl L. Sprague

Lewis Research Center

SUMMARY

The flow and heat-transfer characteristics during the startup of a nuclear rocket are of particular interest because of the bootstrap type of startup. An analytical procedure was assembled using state-of-the-art equations to provide a tool for predicting the transient flow and heat-transfer characteristics of reactor components during the startup.

This report presents the results of applying this analytical procedure to a single thick-walled tube which was selected as typical of a passage in the reflector of a current nuclear reactor. Experiments were performed on a thick-walled tubular test section to provide experimental data for comparison with predicted results. With the test section at room temperature, either liquid-hydrogen or cold-hydrogen-gas flow was directed through the 3/16-inch (0.476-cm) bore of the 55-inch (139.6-cm) long test section until it was thoroughly chilled. During most of the liquid-hydrogen chilldown, a saturated liquid was assumed to be at the inlet of the test section. During the gas chilldown, the inlet gas temperature varied from 470° to 360° R (261° to 200° K). Inlet pressures ranged from 20 to 50 psia (1.38×10^{5} to 3.45×10^{5} N/m^2 abs). The initial wall temperatures and the flow rate, the inlet enthalpy, and the inlet pressure as functions of time from the experimental test were used as input for the analytical procedure.

Comparison of predicted and experimental material temperatures, pressures, and exit temperatures indicated that, when cold hydrogen gas was used as the chilling medium, excellent agreement was obtained. When liquid hydrogen was used, only the average chilldown rates of the test section agreed. Local predicted material temperature variations were traced to characteristics of the heat-transfer correlations used. Pressure and exit temperature variations were related to an extreme sensitivity of predicted values to variations in inlet quality and flow rate.

INTRODUCTION

The bootstrap type startup of a nuclear rocket presents some challenging analytical problems. During the early startup transient, the sensible heat of the components is utilized to vaporize the liquid-hydrogen propellant flowing from a tank. A portion of the vaporized propellant is diverted to power a turbopump which, in turn, drives the system toward design flow and pressure conditions. Reactor power is increased before the component sensible heat is expended, resulting in the attainment of design conditions without the aid of an auxiliary gas-generation system.

The period of bootstrap operation is of sufficient importance to require the formulation of analytical techniques to predict transient heat-transfer and flow characteristics in the various rocket-system components. The specific parameters of interest during transient analysis include

(1) Depth of liquid penetration

(2) Flow distribution in parallel passages

(3) Temperature distribution in the material surrounding the flow passages

(4) Pressure distribution along the length of the passages

The analytical procedure described herein was formulated to calculate the desired parameters during a transient when film boiling or gaseous hydrogen flow occurs in a single passage. The application of this analytical procedure to a parallel-passage case is reported in reference 1. Reference 1 deals with the complex material distribution between passages, the flow distribution between dissimilar passages, and the maldistribution of fluid properties approaching the various passages. The present report deals primarily with the development of the analytical procedure, the selection of correlations, and the influence of various parameters on the predicted results in a single passage.

The thick-walled single tube of this study was selected to simulate the geometry and the heat sink of a typical passage in the reflector of a current nuclear-rocket design.

A literature survey was conducted to determine applicable equations for analysis of the heat transfer and the pressure loss in a thick-walled passage. The conditions of interest include fluid entering the passage as a liquid and leaving as a superheated gas. The survey indicated that various relations are available for flow and heat transfer with a superheated gas. However, for the region marking the transition from high-quality two-phase flow to a gas a few hundred degrees above saturation temperature, there are no recommended equations or experimental data.

Because of questions as to the applicability (and useful range) of some of the correlations, the analytical procedure was assembled in such a fashion that various combinations of equations could be selected and applied. Film-boiling, gaseous-hydrogen heat-transfer, and pressure-drop relations were selected from the literature for use in the analysis, as discussed in appendix B. (Appendix A gives a list of symbols used herein.)

Chilldown experiments were performed to provide experimental data for comparison with results predicted by the analytical procedure. Initial experimental material temperature distribution and experimental schedules of the flow rate and the inlet conditions were used to define the initial and transient conditions for the analysis. The validity and limitations of the analytical procedure are indicated by comparison of predicted and experimentally measured parameters during the transient.

This report, therefore, deals with the following subjects, which, in summation, indicate current capabilities for transient analysis of passages containing two-phase and gaseous hydrogen:

(1) Transient chilldown experiments simulating nuclear-rocket bootstrap conditions. The test section consisted of a flow passage 0.188 inch (0.476 cm) in diameter and 55 inches (139.6 cm) long. The external diameter of the test section was 0.25 inch (0.635 cm) for the first 3 inches (7.62 cm) of length and 0.75 inch (1.9 cm) for the remaining 52 inches (132 cm). The test section was at room temperature at the start of each test. Flow rates ranged up to 0.008 pound per second (0.00363 kg/sec) and inlet pressures ranged up to 47 psia (3.24×10^5 N/m^2 abs).

(2) A description of the analytical procedure. The flow and hydrogen heat-transfer analysis portions of the procedure are described in detail. The interrelation of the flow analysis procedure with previously existing computer routines for evaluation of hydrogen properties and the three-dimensional transient conduction analysis are indicated.

(3) The experimental and analytically predicted transient results are compared and discussed. The characteristics and limitations of currently available heat-transfer equations are indicated.

(4) Examples are presented to illustrate the sensitivity of predicted results to variations in inlet quality (or enthalpy) and flow rate.

APPARATUS

Flow System

The test system is shown schematically in figure 1. Liquid hydrogen, stored in a 300-gallon (1.136 cu m) Dewar, was forced through the system by pressurizing the Dewar with gaseous helium. The piping from the Dewar to the test section and the test section were jacketed to minimize heat leaks. A control valve before the test section was left open for all tests. A three-way valve located just before the test section was utilized for several operational functions. Before a chilldown run, the line to the three-way valve was precooled by liquid hydrogen flowing to the valve and out the vent line. A run was initiated by diverting the flow from the precool position to the run position, where flow

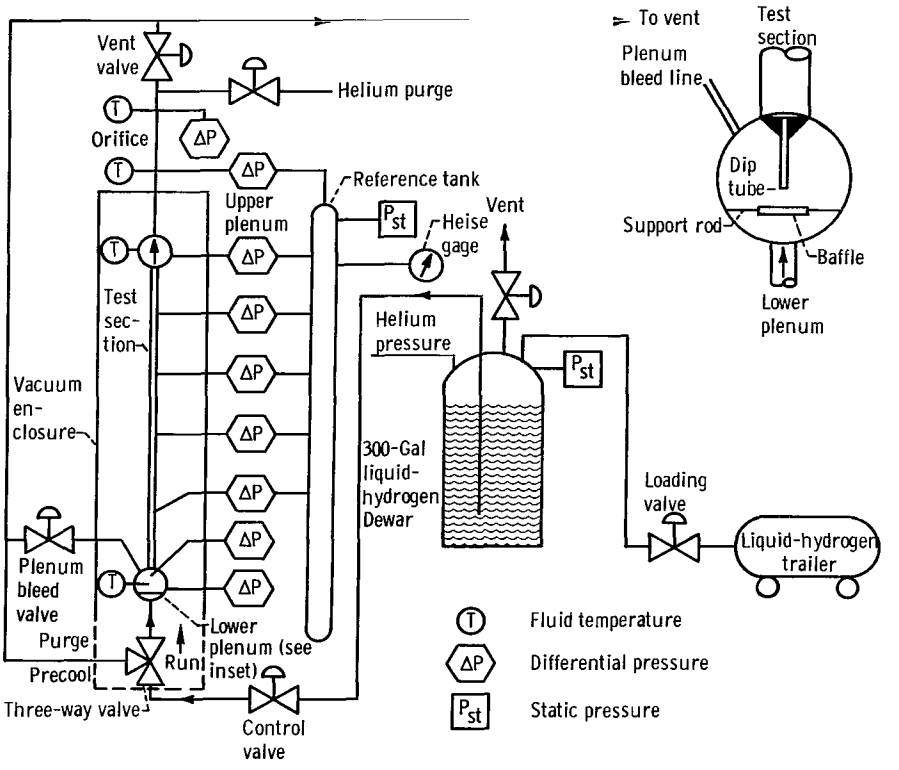

Figure 1. - Schematic drawing of test system.

was directed into the test section. The three-way valve was a ball valve and thus presented no restriction to flow in the run position. After a chilldown run the three-way valve was rotated to connect the test section to the vent line. A helium purge, introduced just before the closed vent valve, was then utilized to reheat the test section to ambient temperature and to permit repetitive testing on a given day.

The lower plenum at the inlet to the test section is shown in the insert in figure 1. This plenum was arranged to separate and bleed off any gas entrained in the liquid and thus to permit only liquid hydrogen to enter the test section. The baffle, a 1/2-inch-diameter (1.27-cm-diam) disk supported by thin rods, prevented the entering liquid from impinging directly on the dip tube. The thin-walled dip tube was welded to the test section. Flow through the plenum bleed valve prevented gas accumulation in the lower plenum. Thus, the liquid level in the lower plenum was kept above the inlet to the dip tube during liquid-hydrogen chilldown runs, except for the first few seconds. Violent boiling from the surfaces of the plenum prevented the formation of a stable liquid-to-gas interface during the first few seconds, until the plenum was chilled. The plenum was a steel cylinder with glass plates on front and back. Liquid flow in the plenum during experiments could be observed through a closed-circuit television system. The test section in the vacuum enclosure and a portion of the system are shown in figure 2.

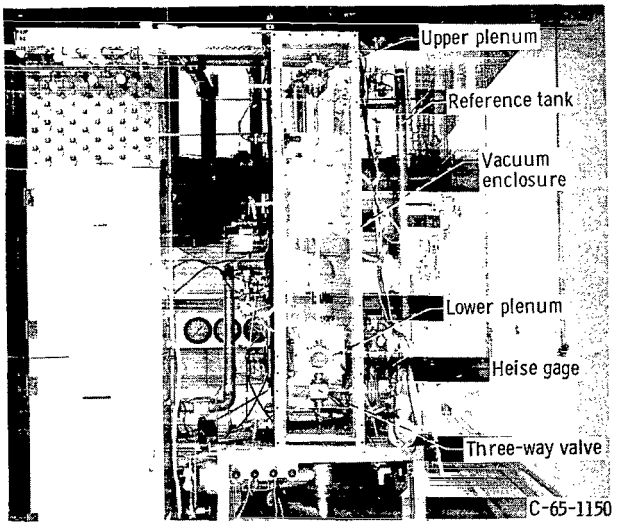

Figure 2. - Single-tube test facility.

Test Section

The 6061-T6 aluminum test section is shown in figure 3. It consisted of two tubes welded together, one 52 inches (132 cm) long with a 0.75-inch (1.905 cm) outer diameter

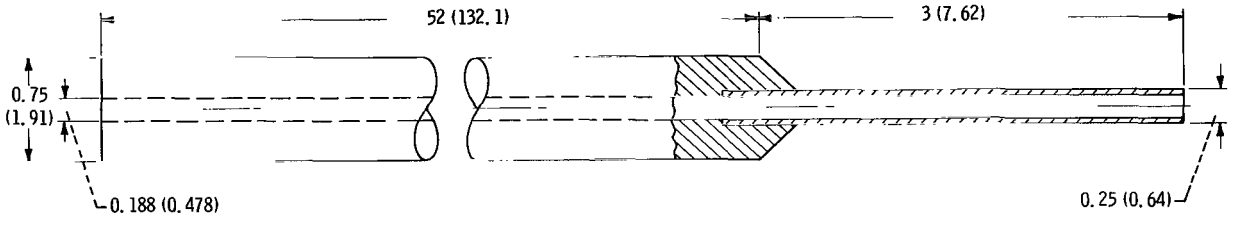

Figure 3. - Test section. (Dimensions are in inches (cm).)

and the other (previously referred to as the dip tube) 3 inches (7.62 cm) long with a 0.25-inch (0.635 cm) outer diameter. The flow-passage diameter was 0.188±0.004 inch (0.478±0.0102 cm) throughout the 55-inch (139.6-cm) length. A slight discontinuity did occur at the junction of the two tubes.

Instrumentation

System fluid pressures were measured at the Dewar, the lower plenum, the upper plenum, and before and across the sharp-edged orifice used for flow measurement downstream of the test section. Fluid temperatures were measured at the lower and upper

plenums and before and after the orifice. The test section was instrumented, as shown in figure 4(a), with 6 static pressure taps and 13 wall-temperature thermocouples spaced along the length.

The copper-constantan thermocouple beads were installed at a depth of 0.176 inch (4.47 mm) from the outer surface, as indicated in figure 4(b) which also presents the dimensions and the tolerances. The installation steps are as follows:

(1) Drill flat-bottomed hole at designated locations.

(2) Run thermocouple bead and insulated leads through aluminum plug. Silver solder bead to copper disk.

(3) Apply thin coating of high-thermal-conductivity silicone grease to lower surface of copper disk.

(4) Press assembly into test section with 300 pounds force (1335 N).

This type of thermocouple installation was selected from several methods considered and screened by analysis and tests to obtain minimum time lag and maximum repeatability. The installation selected represents a compromise to obtain repeatability. Other installations contained an unknown point, line, or surface-contact area between the bead and the surface of interest. The unknown conduction area was evidenced by inconsistent response times within groups of thermocouples installed by other methods. The group installed with copper plugs and silicone grease provided the least spread and compared favorably with the faster responding thermocouples of other groups. The grease fills the void between the surface of interest and the copper disk, providing a maximum-area conduction path to the junction. Reference junctions for all thermocouples were located in 150° F (339° K) reference ovens.

Pressures were measured relative to the pressure in a reference tank (fig. 1). By establishing a positive pressure in the reference tank, the full minus-to-plus range of the differential pressure transducers could be utilized during a run. The use of differential pressure transducers increased the accuracy of measurement as compared with the use of transducers referenced to ambient pressure.

An important feature of this pressure-measurement technique was that it permitted pressure calibrations of the transducer and recording system before and after each run. By closing off the flow system between the three-way valve and the vent valve, the test section could be pressurized to various levels relative to the reference tank. Readings from heise gages on the reference tank and on the purge line were used as reference values. This method of calibration reduced the inconsistencies due to circuit drift that were experienced when differential transducers were referenced to the inlet plenum and could be checked only with electrical calibrations.

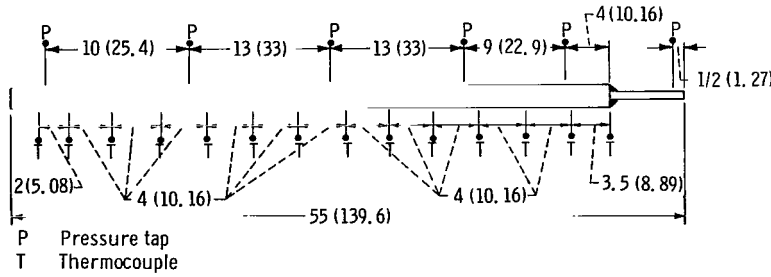

(a) Pressure and temperature measurement locations.

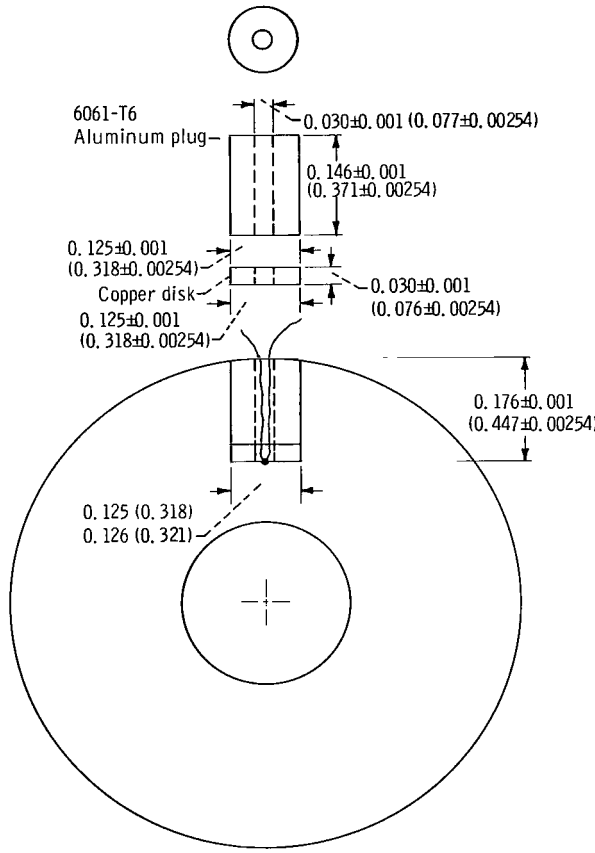

(b) Thermocouple installation.

Figure 4. - Instrumentation locations and installation. (Dimensions are in inches (cm).)

Data Recording

During the runs, the millivolt signals from the pressure transducers and thermocouples were recorded on magnetic tape in a high-speed digital recording system. A digital computer code was utilized to convert the binary millivolt values from the tapes into tabulations of pressure and temperature at the desired time intervals. Time intervals between readings varied from 0.1 second at the start of a chilldown to 1.0 second near the end of a run. Continuous recordings of selected pressure signals were also made on oscillographs to detect flow and pressure oscillations. No significant oscillations were detected during the experimental runs discussed herein.

Measurement Accuracy

Measured parameters, the range of measurements, and the steady-state accuracy are listed in table I. Where possible, an estimate of the time constant is given. The

TABLE I. - ESTIMATED ACCURACY OF MEASUREMENT SYSTEMS

Parameter	Range of measurements	Steady-state accuracy	Time constant, sec
Pressure	1.0 to 30.0 psi; 6.895×10^3 to 2.07×10^5 N/m^2	±2.0 percent of full scale	0.005
Fluid temperature	40° to 550° R; 22.2° to 306° K	$\pm15^\circ$ R; $\pm8.3^\circ$ K	.2
Wall temperature	100° to 550° R; 55.5° to 306° K	$\pm5^\circ$ R; $\pm2.78^\circ$ K	-----
Flow rate	0 to 0.015 lb/sec; 0 to 0.0068 kg/sec	±2 percent	.2

values listed reflect consideration of basic instrument accuracy, the environment of the transducer, and the accuracy of the signal conditioning and recording systems. The heise gage used as a reference for pressure-transducer signal calibration was accurate to ±0.05 psi (±345 N/m^2) in the range considered. By instrumenting the test section with wall-temperature thermocouples from a single spool of wire, the steady-state spread between thermocouples was held below 2° R (1.1° K).

When two-phase hydrogen was entering the test section, the inlet enthalpy could only be estimated. The measured inlet pressure and temperature are not sufficient to define the enthalpy. Visual observation (by closed-circuit television) provided only a gross indication of whether the fluid was predominately liquid or gas. Although the inlet plenum was designed to separate the phases, the estimate of the enthalpy of the hydrogen entering the test section was the greatest source of inaccuracy.

EXPERIMENTAL PROCEDURES

Cold Gas Runs

Cold gas runs were made to provide transient chilldown data for comparison with predicted results without the variables introduced by two-phase hydrogen. The run procedure was unique in that the sensible heat stored in the walls of the Dewar and transfer lines was used to vaporize liquid parahydrogen flowing from the supply trailer (fig. 1). The procedure was as follows:

(1) Precooling: Flow was initiated by pressurizing the supply trailer and opening the loading valve. Flow proceeded through the Dewar and was vented at the three-way valve (precool position).

(2) Run: When the three-way valve had cooled to 460° R (256° K), an electric timer was energized, which then sequenced the events of the run. The vent valve and the plenum bleed valve were opened, and the recording system was turned on. The actual run started when the three-way valve diverted the flow from the vent to the test section (run position). An event marker signal was started when flow was directed into the test section. At the end of a run, the sequence was reversed, except that the vent valve was left open.

Liquid Runs

The procedure for a typical liquid-hydrogen chilldown run is as follows:

(1) Precooling: The Dewar was pressurized, the control valves were opened, and the three-way valve was set in the precool position. Flow was maintained until a thermocouple on the three-way-valve body indicated liquid-hydrogen temperature.

(2) Venting: The Dewar was vented to the atmosphere, and the fluid in the Dewar was allowed to reach saturation conditions. This procedure caused the fluid to be slightly subcooled when the Dewar was pressurized.

(3) Prerun: The Dewar was pressurized, and flow was started with the three-way valve in the precool position.

(4) Run: After precooling for 10 seconds, the timer was energized, and the sequence explained for the gas run was followed.

After each run, the test section could be reheated by purging with gaseous helium at ambient temperature. The test section was then allowed to stabilize to a constant wall temperature before another liquid run was made.

ANALYTICAL PROCEDURE

General Description

A description of the analytical procedure as applied to the single thick-walled tube is presented. The procedure was formulated to be applicable to the analysis of the more complex components of the nuclear rocket. Satisfying this objective required that the specification of the geometry of the component or the test section be retained as input. Also, several heat-transfer correlations were included in the body of the code and various combinations were selected by input calls to permit the evaluation of various correlations as extrapolated to cover the range of conditions.

The single thick-walled test section was divided into fifty-five 1-inch- (2.54-cm-) long increments, as indicated in figure 5(a). The material surrounding the flow passage in each length element was in turn divided into concentric rings or volume elements. A single 0.0312-inch-thick (0.79-mm-thick) ring was sufficient for each length element for the first 2 inches (5.08 cm) of thin-walled tubing. The third length element was 0.0337 inch (0.856 mm) thick to account for the weld fillet (as shown in fig. 5(a)). The material in each of the remaining 52 elements was divided into four concentric rings each 0.0702 inch (1.78 mm) thick (as illustrated in fig. 5(b)). The material was considered as pie-shaped segments, and parallelepiped elements were defined to represent each concentric ring (fig. 5(c)) because of symmetry. These volume elements were specified as geometry input to the three-dimensional transient heat-conduction section (TØSS) (ref. 2) of the analytical procedure, while the flow-passage diameter and the length element were specified as geometry input to the flow analysis (FLØW) portion of the procedure.

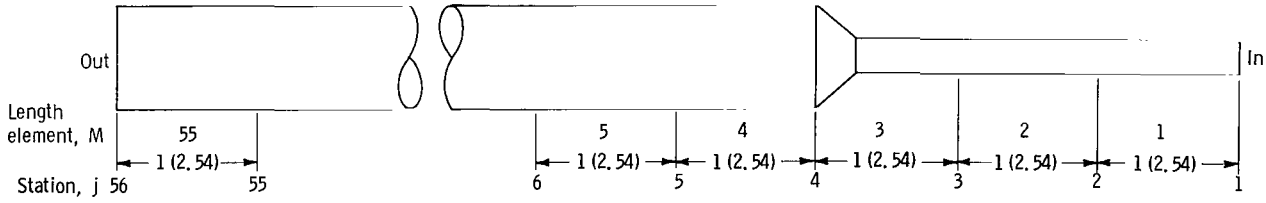

(a) Distribution of length elements and stations (in and out).

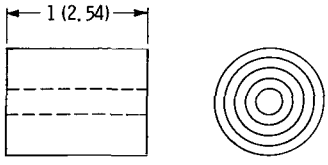

(b) Distribution of material into rings of equal thickness.

(c) Illustration of node size using symmetry.

Figure 5. - Single thick-walled test section. (Dimensions in inches (cm).)

A block diagram showing the three major routines of the computer program involved in the analytical procedure is shown in figure 6. The input pertinent to each routine and the interrelation of one routine with another are indicated. The three routines are STATE (see ref. 3), FLØW, and TØSS. The analytical procedure was formulated by utilizing two existing routines, STATE and TØSS, developing FLØW, and combining the three.

The subroutine STATE is a hydrogen-properties library. Given either values of pressure and enthalpy in the two-phase region or values of pressure and temperature in the gas region and the para-ortho composition (100 percent para for this study), STATE returns the appropriate fluid properties (ρ, μ, C_p, k, etc.) as required, for the flow and heat-transfer analysis performed in FLØW. (See appendix A for a complete list of symbols.)

As mentioned previously, TØSS is a three-dimensional transient heat-conduction routine. In this analytical procedure, the TØSS routine receives heat-transfer coefficients and bulk temperatures for each length element from the FLØW routine, calculates the change in material-temperature distribution over a time increment, and returns the final surface-temperature distribution to FLØW. For this application, TØSS was modified to use temperature-dependent properties for the material-thermal conductivity and specific heat.

The function of FLØW in the analytical procedure is basically to determine the heat-transfer coefficients, the pressure, and the enthalpy along the length of the passage

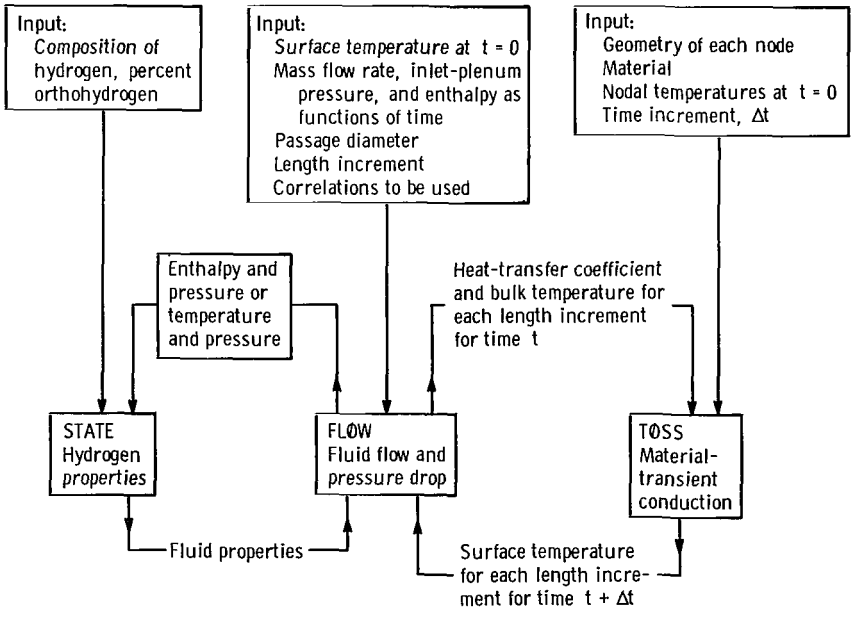

Figure 6. - Block diagram of transient analysis procedure showing input and interrelation of three basic routines.

(length element by length element) when given flow rate, inlet pressure, inlet enthalpy, and surface-temperature distribution. The routine FLØW performs a steady-state analysis assuming continuity. Flow rate and inlet conditions are defined periodically during the transient, and the conditions defined are assumed to be valid over a time period Δt.

A time increment Δt is assumed. Input for FLØW consists of surface temperature defined at $t = t_i$ and inlet pressure, inlet enthalpy, and flow rate defined at the time $t_i + (\Delta t/2)$ which represents average conditions for the first time increment. The material temperatures at $t = t_i$ are input to TØSS. The routine TØSS receives the heat-transfer coefficients and bulk temperatures from FLØW evaluated at $t_i + (\Delta t/2)$ and determines the change in material temperatures in the time period from $t = t_i$ to $t_i = t_i + \Delta t$. Surface temperatures for $t = t + \Delta t$ are returned to FLØW, and the system is ready for the next time increment. Studies were made using time increments of 0.1 second, which checked within 0.1 percent of the values obtained with a 1.0-second time increment. Because of this, the errors introduced by using a quasi-steady-state approach were considered to be negligible for the rate of change of the variables being considered, and a time increment of 1.0 second was used for this study. Longer time increments were not investigated but could lead to error.

Description of FLØW

The calculation procedure flow chart shown in figure 7 is discussed in this section. The input, block 1, was discussed in connection with figure 6 in the preceding section. The inlet fluid conditions are considered as total values because the plenum area is large compared with the flow-passage area. In block 2, static pressure and enthalpy at station $j = 1$ (see fig. 5(a)) are calculated by using equations (1) and (2) and assuming $\rho_{j=1} = \rho_{in}$:

$$P_{j=1} = P_{in} - \left[(1 + K') \frac{G^2}{2g\rho_{j=1}}\right] \frac{1}{144} \tag{1}$$

(where K' is an entrance pressure loss coefficient (ref. 4) equal to 0.2 for this study)

$$H_{j=1} = H_{in} - \frac{G^2}{2gJ\rho_{j=1}^2} \tag{2}$$

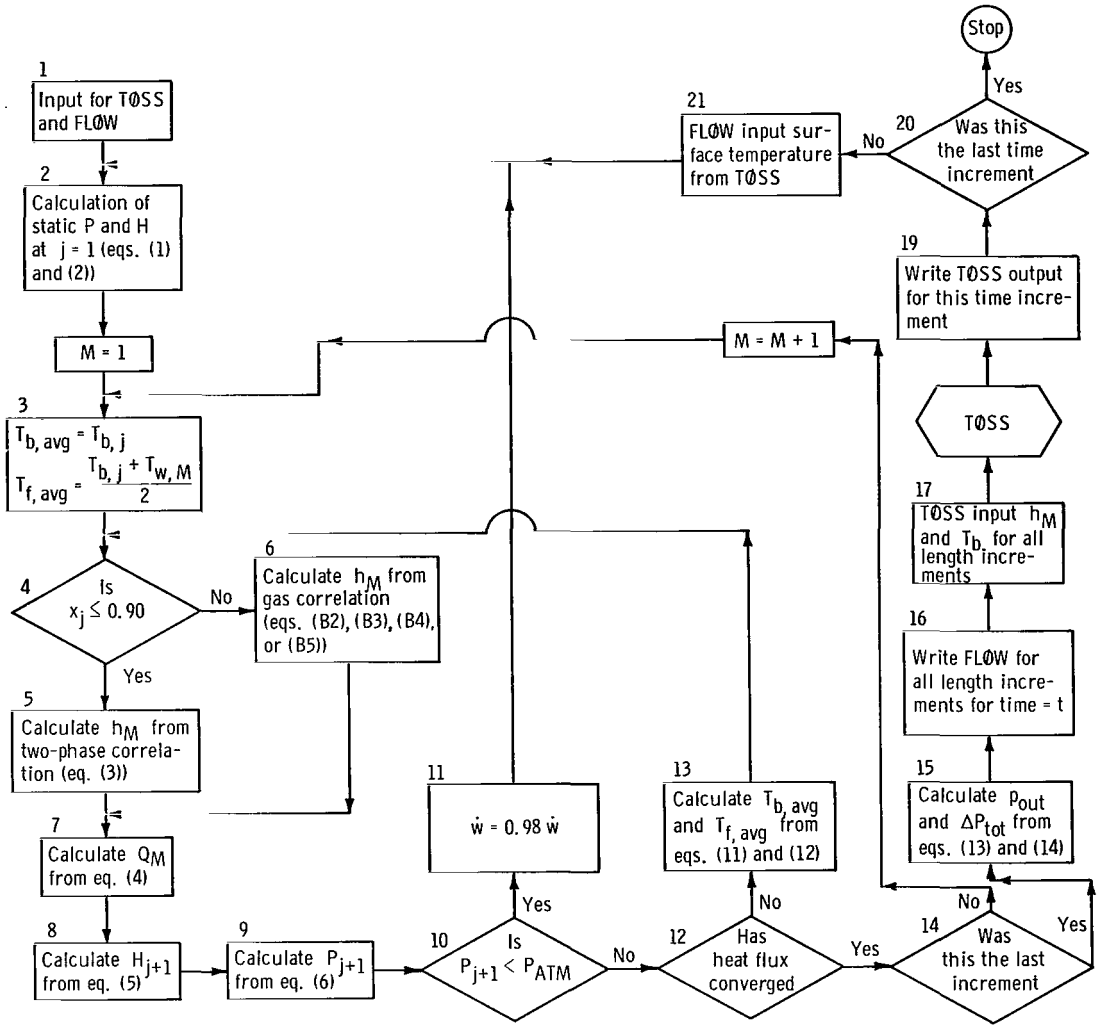

Figure 7. - Flow chart for analytical procedure.

Blocks 1 and 2 provide the necessary input to enter the heat-transfer and pressure-drop analysis loop (blocks 3 to 13) for the length element $M = 1$.

As this is an iterative loop, it is helpful to remember that the important unknowns to be evaluated are the $T_{b,av}$ and h_{av}, which are required for TØSS, and also $H_{(j+1)}$, which is required before progressing to the next length element. Actually, by converging on the incremental heat flux Q_M required to evaluate $H_{(j+1)}$, all other unknowns are determined.

Block 3 provides trial values for the average bulk and film temperatures for the length element with the assumption that the bulk temperature at j is equal to that at $j + 1$ for the first iteration.

Block 4 contains a test of inlet quality. Inlet quality is obtained in STATE from values of H_j and P_j. Because STATE provides fluid properties to nearly all blocks,

its presence should be understood even though it is not shown. If inlet quality is less than or equal to 0.9, a two-phase heat-transfer equation is used to obtain h_M (block 5). If the inlet quality is greater than 0.9, a gas-heat-transfer equation is used (block 6). (See appendix B for further discussion of these equations.)

If for this discussion it is assumed that the quality is less than 0.9, the heat-transfer coefficient is determined by solving the following equation from reference 5:

$$h_M = 0.023 \frac{k_f}{D} \left(\frac{Re_{tp}^{0.8} Pr_f^{0.4}}{0.611 + 1.93 X_{tt}} \right) \tag{3}$$

where

$$Re_{tp} = \frac{GD}{\mu_f} \frac{\rho_{fm}}{\rho_b}$$

$$\rho_{fm} = \frac{1}{\frac{x}{\rho_f} + \frac{1 - x}{\rho_l}}$$

$$\rho_b = \frac{1}{\frac{x}{\rho_g} + \frac{1 - x}{\rho_l}}$$

$$X_{tt} = \left(\frac{1 - x}{x} \right)^{0.9} \left(\frac{\mu_l}{\mu_f} \right)^{0.1} \left(\frac{\rho_f}{\rho_l} \right)^{0.5}$$

The heat transferred to the fluid in length element M is then evaluated in block 7 from the equation

$$Q_M = h_M A_{s,M} (T_w - T_b) \tag{4}$$

The enthalpy at $j + 1$ is evaluated from a form of the general energy equation (block 8)

$$H_{j+1} = H_j + \frac{Q_M}{\dot{w}} + \frac{G^2}{2gJ} \left(\frac{1}{\rho_j^2} - \frac{1}{\rho_{j+1}^2} \right) \tag{5}$$

The static pressure (block 9) at $j + 1$ is obtained from

$$P_{j+1} = P_j - \Delta P_{fr} - \Delta P_{mom} - \Delta P_{res} \tag{6}$$

where

$$\Delta P_{fr} = \left(4f \frac{\Delta l}{D} \frac{G^2}{2g \frac{\rho_j + \rho_{j+1}}{2}} \right) \frac{1}{144} \tag{7}$$

and

$$f = \frac{T_b}{T_f \left[4.0 \log \left(Re_f \frac{\rho_f}{\rho_b} \sqrt{f \frac{T_b}{T_f}} \right) - 0.4 \right]^2} \tag{8}$$

where

$$Re_f = \frac{GD}{\mu_f}$$

(ref. 6). Equation (8) is solved by an iterative method. The momentum component of pressure drop is evaluated from

$$\Delta P_{mom} = \frac{G^2}{g} \left(\frac{1}{\rho_{j+1}} - \frac{1}{\rho_j} \right) \frac{1}{144} \tag{9}$$

If there is a restriction in the length element, the pressure loss due to the flow restriction is calculated from the equation

$$\Delta P_{res} = \frac{K\dot{w}^2}{A_{res}^2 2g \left(\frac{\rho_j + \rho_{j+1}}{2} \right)} \frac{1}{144} \tag{10}$$

where K is either determined experimentally or estimated from tabular data such as presented in reference 7. In this study, the coefficient was determined experimentally to be 0.43.

In block 10, a test is made to see if P_{j+1} is realistic. If P_{j+1} is too low, the flow rate is reduced by 2 percent (block 11), and the analysis starts again at block 2. The reason for this reduction of flow is discussed in the section RESULTS AND DISCUSSION.

In block 12, a test is made to see if the heat flow Q_M has converged. During the first iteration, there is no prior value with which to make a comparison. Therefore, block 12 is bypassed, and the procedure goes to block 13. During succeeding iterations, a test is made, and, if the calculated Q_M is within 0.1 percent of the previously calculated value, the calculations proceed to block 14.

If the heat flux has not converged, the calculations proceed to block 13, where the average bulk and film temperatures are calculated from the following equations:

$$T_{b,av} = \frac{T_{b,j} + T_{b,j+1}}{2} \tag{11}$$

$$T_{f,av} = \frac{T_w + T_{b,av}}{2} \tag{12}$$

where $T_{b,j+1}$ is obtained from the P_{j+1} and H_{j+1} using the subroutine STATE. The loop then starts again at block 4 and continues until the heat flow converges in block 12.

In block 14, the number of the length element is checked. If M is less than the total number of increments, the procedure is directed to analyze the next length element M + 1 using the exit station conditions from the previous length element as inlet station conditions. If the last length element has been analyzed, the analysis moves to block 15.

In block 15, the pressure in the exit plenum is calculated from

$$P_{out} = P_n + \left[(1 - K'')\frac{\rho_n V_n^2}{2g}\right]\frac{1}{144} \tag{13}$$

$$\Delta P_{tot} = P_{in} - P_{out} \tag{14}$$

The K'' term in equation (13) is evaluated by using the following relation (ref. 7):

$$K'' = \left(1 - \frac{D_n^2}{D_{out}^2}\right)^2 \tag{15}$$

Block 17 can be considered as a storage area for values calculated by FLØW.

Block 18 is TØSS, which accepts bulk temperature and heat-transfer coefficients for the length elements and calculates the change in material temperatures over the time increment. Block 19 can be considered as a storage area for values calculated by TØSS. Block 20 tests to see if the analysis covers the intended time period. Block 21 provides the required input for the next FLØW calculation.

Output: The desired information stored in blocks 16 and 19 is printed out in tabular form for each time increment. This output includes pressures, bulk temperatures, heat flow, and the material temperature in the incremental volume rings.

The FLØW routine can be used independently of TØSS for predicting instantaneous flow conditions. The input to FLØW is the same as for transient conditions. Without TØSS there is no transient feature or time parameter. FLØW merely calculates the flow characteristics which satisfy the input conditions. Blocks 1 to 16 represent the steady-state version of FLØW.

FLØW was used to perform the parametric study reported in reference 8. During that study, the influence of changes in flow rate, inlet quality, and wall temperature on overall pressure drop and heat transfer in a passage were evaluated. A similar study is included in this report to evaluate variations caused by measurement inaccuracies in determining inlet conditions.

METHOD OF COMPARING PREDICTED AND EXPERIMENTAL RESULTS

The flow rate, inlet conditions, and initial wall temperatures for the predicted chill-down run correspond to the experimental run with which it is to be compared. Other parameters must be considered in determining whether the transient prediction technique gives a valid reproduction of the physical process.

A comparison of the predicted and experimentally measured exit fluid temperatures during the transient gives an indication of the accuracy with which the overall heat transfer to the fluid is being predicted. The accuracy of predicted local heat-transfer rates is indicated by curves showing the relation between predicted and measured material temperatures along the length of the test section at various times during the transient.

Because the fluid pressure drop through the channel is a function of the heat transfer, curves comparing the predicted and measured pressure drop from the inlet to the outlet of the channel provide another indication of the merit of the various heat-transfer equa-

tions. Curves of predicted and measured local pressures along the length at various times during the transient permit comparison of local conditions.

In general, these four types of curves, exit fluid temperature against time, material temperature against length at various times, overall pressure drop against time, and local pressure against length, are presented herein for the two runs to permit comparison of predicted and experimental results. Additional figures are included as required to substantiate the discussion of the basic figures.

RESULTS AND DISCUSSION

Experimental Values Used as Input to Analytical Procedure

Several chilldown experiments were performed. Two experimental runs (one gas and one liquid) are presented in this report as typical of the others and are compared with the results predicted by the transient-analysis procedure. Experimental data for two other liquid runs are presented in appendix C for those who wish to perform transient analysis with future correlations.

The experimental data required as input to the transient-analysis procedure are the flow rate, the inlet pressure, and the inlet enthalpy as functions of time, and also the

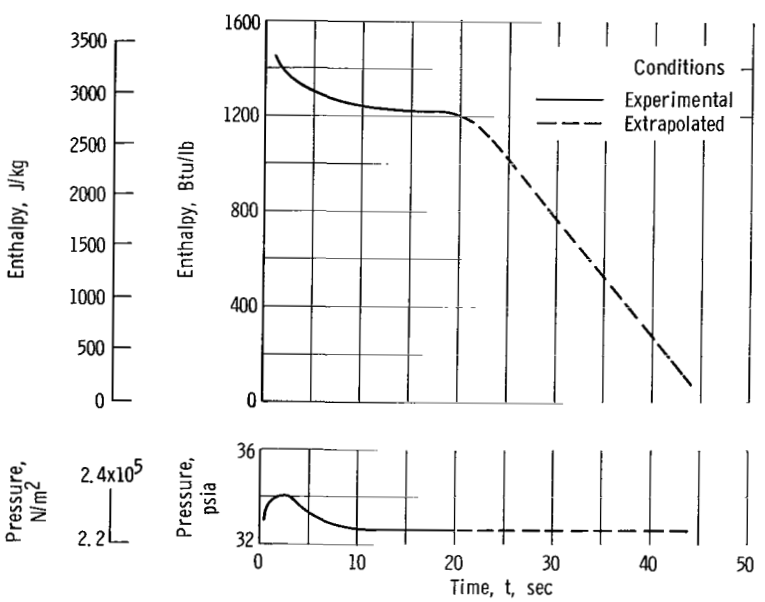

Figure 8. - Initial and inlet flow conditions for gas run. At zero time, material temperature is constant at 522° R (290° K). Flow rate, 0.00235 pound per second (0.001066 kg/sec).

material temperatures throughout the test section at time $t = t_i$. The necessary input data for a chilldown run with gaseous parahydrogen entering the test section are provided in figure 8. Although the inlet pressure and enthalpy change with time, the flow rate remained constant throughout the 20 seconds that data were recorded. The dashed segments of the curves represent an extrapolation to provide colder inlet gas temperatures for comparison of correlations. The initial material temperature was a constant 522° R (290° K) along the length.

The necessary input data for a chilldown test with liquid hydrogen entering the test section are provided in figure 9. The material temperature again was a constant 522° R (290° K).

Figures 8 and 9 represent a "best interpretation" of the experimental conditions. Accuracy has been discussed previously in the section APPARATUS, and the sensitivity of predicted results to inaccuracies is discussed in the section Inlet quality and flow-rate variation effects at 5.0 seconds. Redundant instrumentation was used at various locations in the system, but, as sometimes happens, the measurements did not always complement

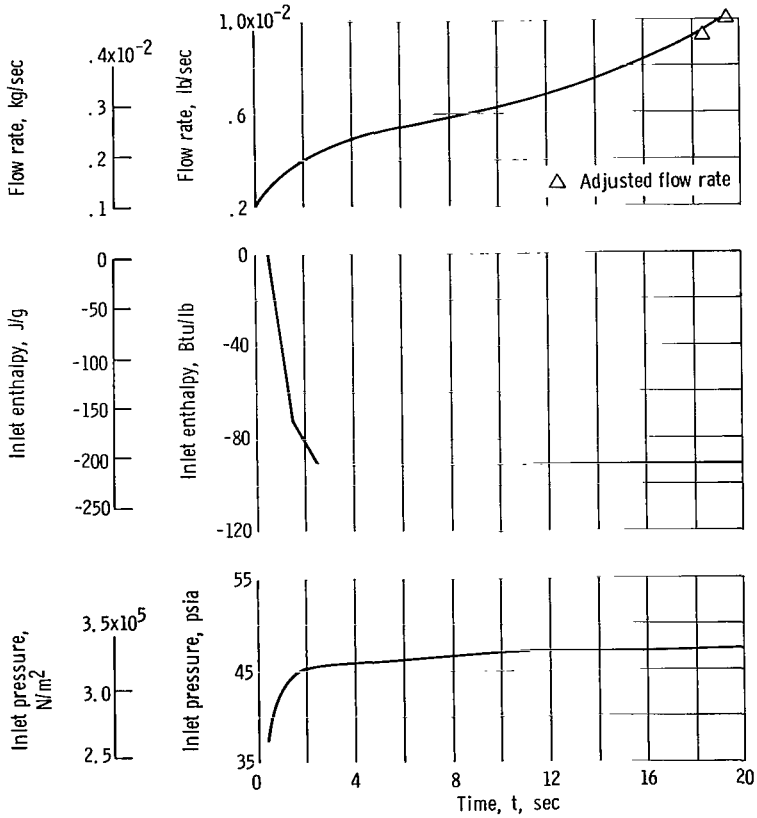

Figure 9. - Initial and inlet flow conditions for liquid run. At zero time, material temperature is constant at 522° R (290° K).

each other. As an example, both carbon resistors and fine-wire copper-constantan thermocouples were located in the inlet plenum to measure fluid temperatures. When liquid hydrogen entered the plenum, the thermocouple started indicating liquid-hydrogen temperature almost immediately, while the carbon resistor would take up to 5 seconds to reach liquid temperature. The carbon resistor had been carefully calibrated in a cryostat and was considered more accurate than the thermocouple. However, the long response time of the carbon resistor negated its use in transient work.

Gas Run

The gas run was analyzed first to evaluate the basic logic of the computer code and second to obtain a comparison of the experimental and predicted transient characteristics using each of four gas heat-transfer equations without the complexity of considering two-phase flow. The first objective was verified by a careful study of the predicted longitudinal and radial temperature profiles in the material, the pressure gradients, the fluid property changes with length, etc. to determine if logical characteristics were obtained. The curves used in verifying the logic of the analytical procedure were similar to those used in evaluating various heat-transfer-coefficient equations and are not reproduced herein. The curves that are included indicate that predicted pressure gradients and temperature gradients are in the proper directions and that peculiar changes in parameters with length or time are traceable to the characteristics of the equations used.

Overall characteristics. - The exit fluid temperatures as calculated with the four equations are compared (fig. 10) with experimental values during the transient. Considering first the predicted exit temperatures, it may be noted that the maximum spread between various heat-transfer equations in the first 20 seconds of the transient is 5° R (2.78° K). The fact that the fluid entering the passage was at the same temperature at a given time for all calculations and that the fluid leaving was calculated to be nearly the same indicate that all four correlations give the same overall heat-transfer rates within ±5 percent.

The various predicted exit temperatures retain approximately the same interrelation while diverging slowly with time. The highest overall heat-transfer rates are obtained with equation (B3). The lowest are obtained with equation (B4), which provides rates approximately 4.5 percent lower than equation (B3).

All predicted exit temperatures are 5 to 10 percent lower than the experimentally measured exit temperatures. The total spread, including the experimental values, is 10° R (5.56° K) or less.

In the extrapolated range, the predicted exit temperatures retain approximately the same relative position with time, although temperatures predicted by equations (B4) and

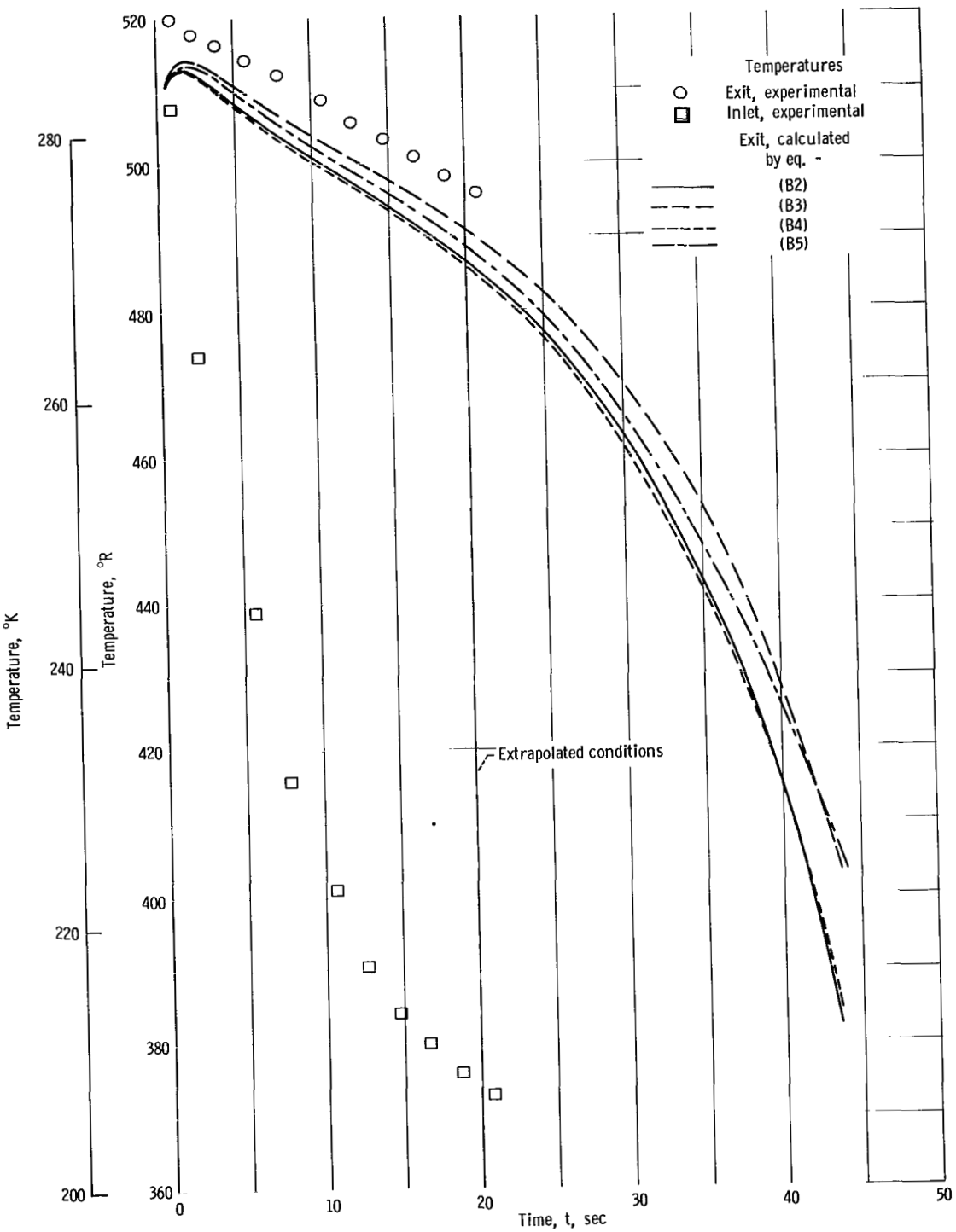

Figure 10. - Comparison of experimental and calculated exit fluid temperatures using various heat-transfer correlations. Gas run.

(B5) increased slightly relative to the other two predicted temperatures. Equation (B5) uses constant fluid properties. The deviation caused by this property assumption is surprisingly small.

Arbitrary extrapolation rates equal to one-half and twice that presented in this report were investigated. The magnitudes and trends were similar to those reported herein.

Figure 11 presents a comparison of predicted and measured pressure drop through the passage during the transient. The predicted values all cluster within a 3-percent spread and are slightly lower than the experimental values. Similar trends indicated by the same relative position of predicted curves in figures 10 and 11 reflect the strong influence of the heat-transfer rate on the calculated pressure drop.

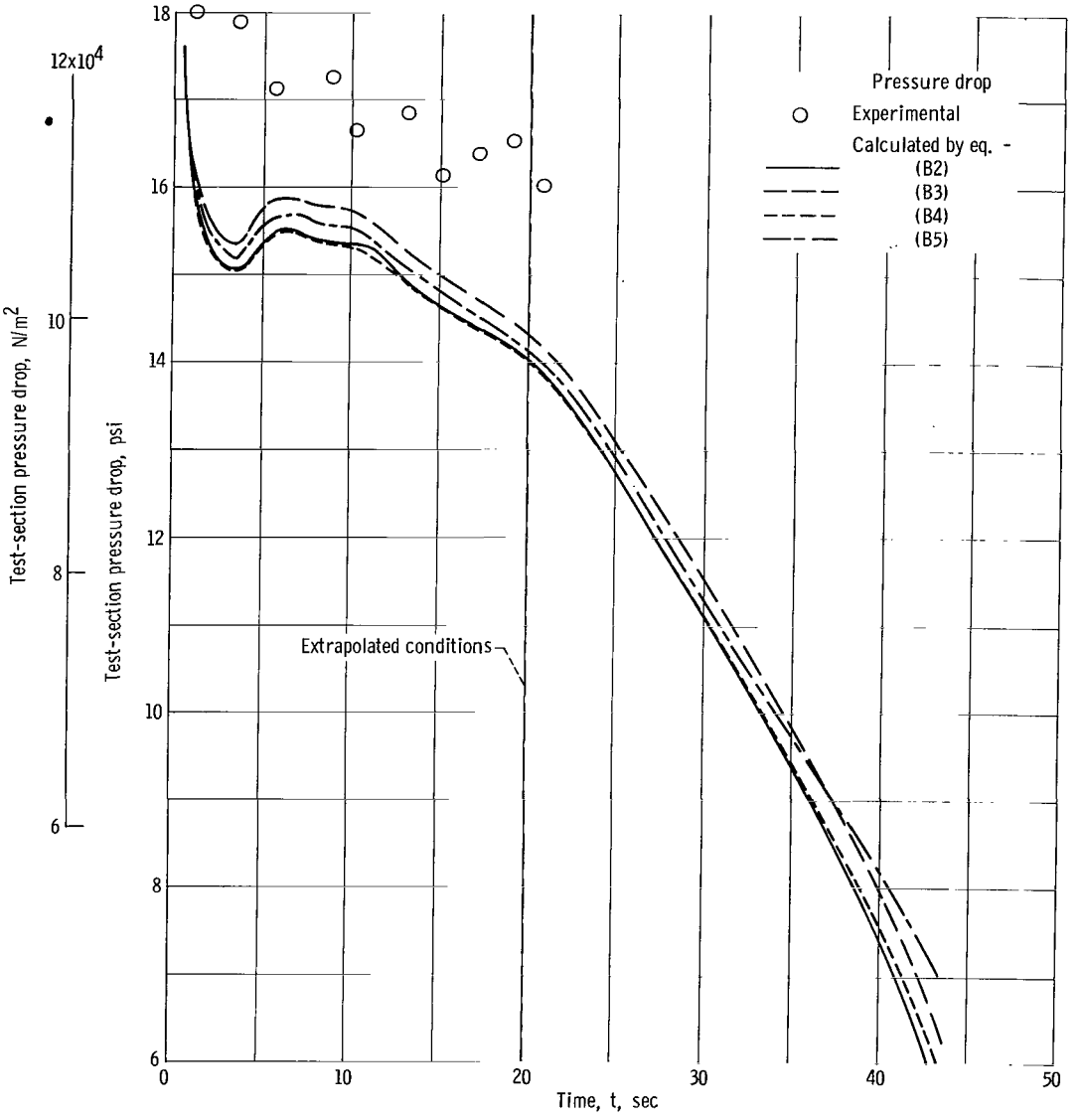

Figure 11. - Comparison of experimental and calculated pressure drop across test section using various heat-transfer correlations. Gas run.

Local characteristics. - An indication of the validity of predicted local heat-transfer rates may be obtained by comparing the predicted material temperature along the length with the experimental values.

Figure 12(a) presents a comparison of the experimental wall temperatures with those predicted using equation (B3) at 5, 10, 20, and 30 seconds during the transient. The zero-time experimental values are the initial conditions for the analysis.

The 3-inch-long (7.62-cm-long) thin-walled dip tube chilled down very rapidly, and conduction to this section strongly influenced the nearby material temperatures. The temperatures plotted represent the centers of the single volume elements in the first 3 inches of length and the centers of the second volume elements of the flow passage for the remainder of the passage. The centers of these volume elements in the thick-walled

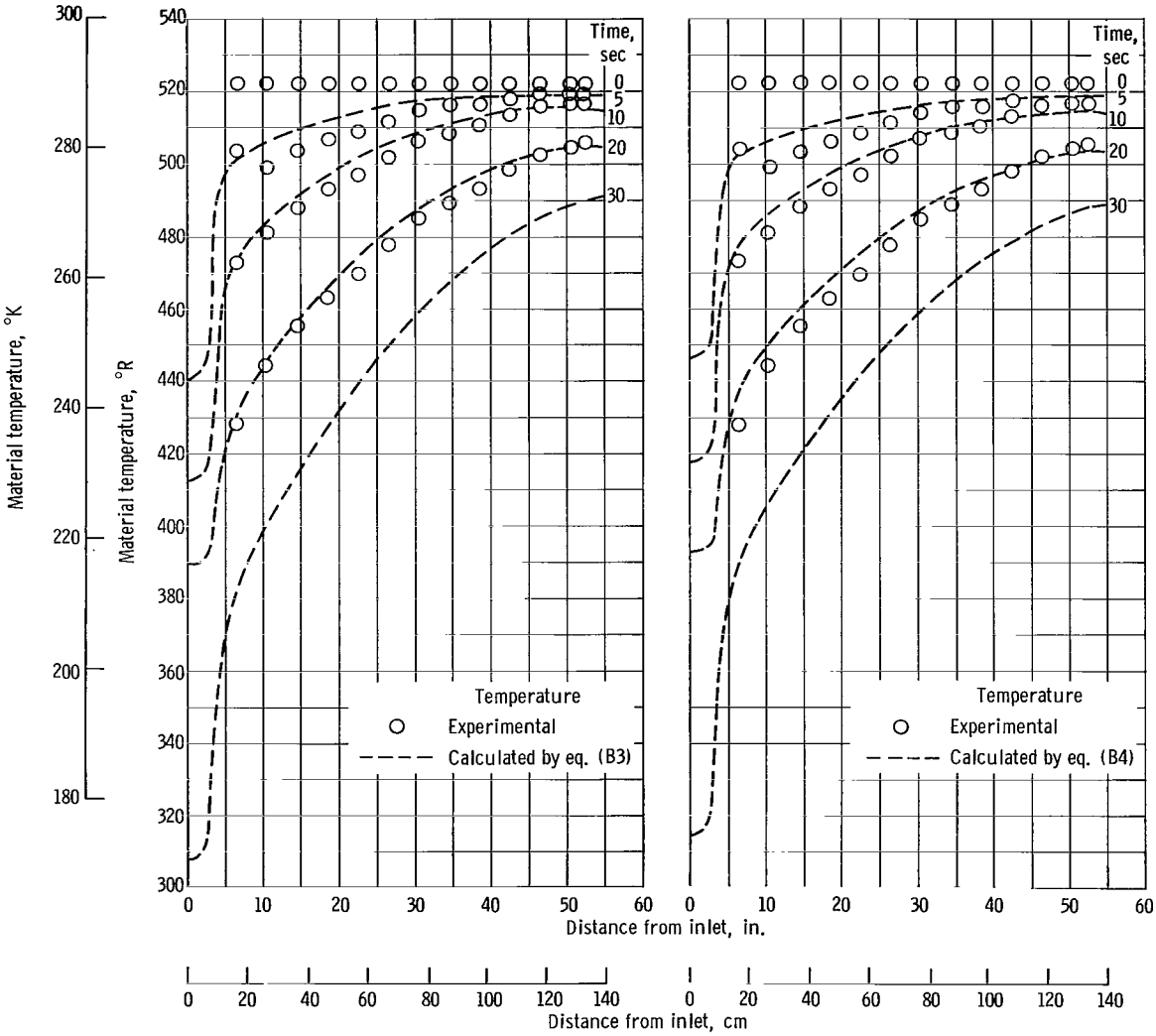

(a) Comparison of experimental data with equation (B3). (b) Comparison of experimental data with equation (B4).

Figure 12. - Axial material temperature profile. Gas run.

portion correspond to the radial location of the thermocouple beads. The thermocouple at the 6.5-inch (16.5-cm) station was later found to be loosely installed, which accounts for its lag with time.

Equation (B3) provides the highest overall heat-transfer rate, as discussed previously. The predicted material temperatures for this run were all within 7° R (3.89° K) of the experimental values. Equation (B3) contains an entrance term (i.e., $1 + 0.3(D/L)^{0.7}$) which increases the heat-transfer coefficient by approximately 15 percent in the first length element and asymptotically approaches 1 as the distance from the entrance increases. In the tenth length element, this term has less than a 2-percent effect.

Figure 12(b) contains a comparison of material temperatures predicted by using equation (B4) with experimental values. Equation (B4) produced the lowest overall heat-transfer rates; however, the predicted material temperatures are still all within 7° R (3.89° K) of the experimental value. The L/D term in equation (B4) is of the form $C = 0.29 + 0.0019$ L/D, where C is the negative exponent of the T_w/T_b ratio. This

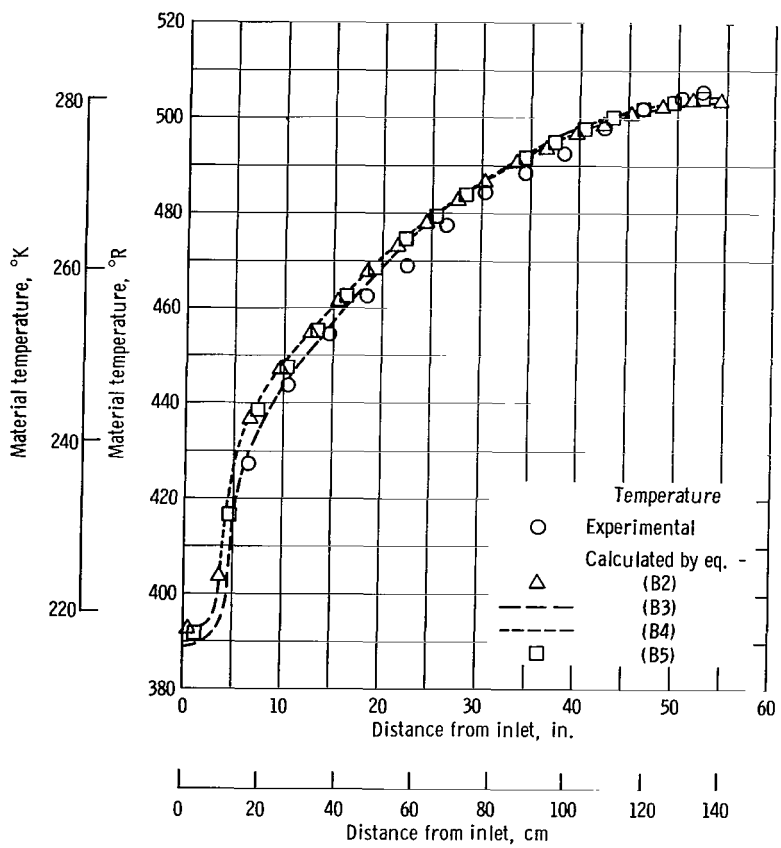

(c) Comparison of experimental data with gas correlations at 20.0 seconds.

Figure 12. - Concluded.

term enhances the heat-transfer coefficient with increase in distance from the entrance. This effect is reflected in figure 12(b) by the fact that the predicted temperatures near the exit of the passage tend to lead the experimental values, indicating slightly higher local heat-transfer rates in this region. The L/D term in equation (B4) does not apply to entrance effects.

Figure 12(c) presents a composite of the experimental and predicted material temperatures at 20 seconds. The dashed and solid curves represent results obtained with equations (B3) and (B4), respectively, and the crossover results from the differences in the L/D terms. Results from using equations (B2) and (B5) are included and generally fall between the values obtained by equations (B3) and (B4).

Figure 13 presents the predicted radial material temperature profiles at four longitudinal positions of the thermocouples. Predictions obtained by using equations (B3) and (B4) were used. The predicted change in material temperature from flow surface to exterior was less than 3^{o} R (1.67^{o} K).

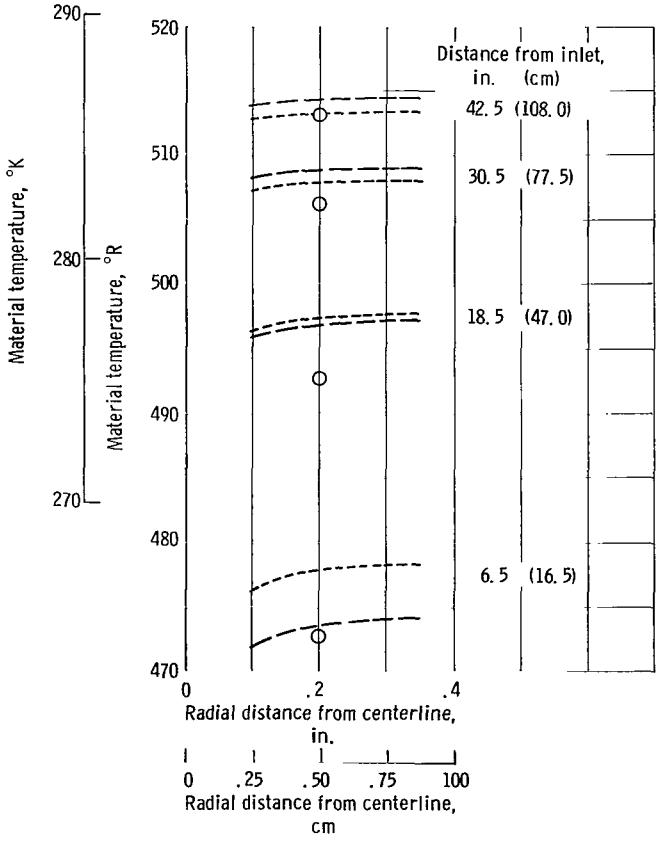

Figure 13. - Comparison of experimental with calculated radial temperature profiles at 10 seconds. Gas run.

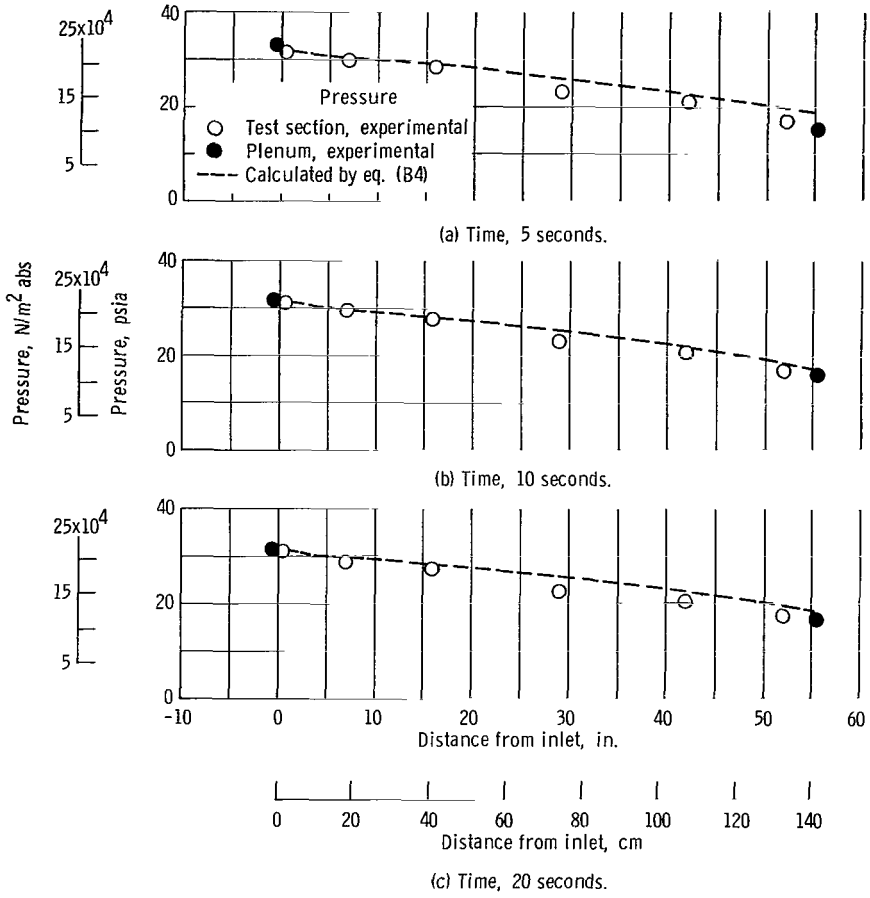

Figure 14. - Comparison of experimental and predicted pressures along test section at 5, 10, and 20 seconds. Gas run.

Figure 14 presents the predicted and experimental pressures along the length of the test section. The solid symbols denote inlet and exit plenum pressures, and the open symbols denote measured static pressures along the length. The experimental values indicate the same trend but slightly more pressure drop than the predicted values. This result indicates again that the correlations used predict less heat transfer, and therefore less pressure drop, than was indicated experimentally. Loss coefficients at the entrance and at the transition between tubes were determined experimentally from isothermal nitrogen gas calibrations of the test section.

Liquid Run

Transient analysis of the chilldown of the test section was much more difficult with liquid or two-phase hydrogen than with cold gas. The difficulty was partly attributed to

the extreme sensitivity of the predicted results to inlet conditions (inlet pressure, enthalpy, and flow rate).

Within the range of experimental accuracy for determining inlet conditions for transient analysis, there were combinations of values which were incompatible with realistic results. These incompatible combinations of inlet values became immediately apparent during early efforts at transient analysis. The analytical procedure would calculate excessive pressure losses in the passage and would then stop. The minimum acceptable static pressure in the passage had been established as the ambient barometric pressure. This minimum had been selected on the assumption that the exit-orifice and vent-stack losses should provide sufficient back pressure to keep the pressures in the test section above atmospheric pressure.

A study was made of the effect of inlet parameters on the overall pressure drop in the passage and on the overall heat transfer to the fluid. Wall temperatures were assumed to be constant in this study, a portion of which is reported in reference 8. As a result of that study, a flow-rate reduction loop was added to the analytical procedure. This feature was fixed to permit the procedure to continue through the transient. Each time a pressure lower than barometric was calculated in the passage the flow rate was reduced by 2 percent, and the flow analysis would start again at the inlet to the passage for that time increment.

Two other loops and combinations thereof were evaluated but are not included in the analytical procedure presented herein. One of the loops merely increased the inlet pressure if pressure at any station was too low. The other loop required an additional experimental parameter as input, the test-section exit fluid temperature. This loop compared the calculated and experimental exit fluid temperatures, calculated the difference in terms of enthalpy, and readjusted the inlet enthalpy by an amount proportional to the difference. The loops involving flow-rate and inlet pressure adjustments were equally effective in permitting transient analysis over the chilldown period. The loop involving an inlet enthalpy correction required one of the other two loops to permit analysis to proceed to the end of the test section without stopping because of low calculated pressures. If the precision of the heat-transfer correlations was beyond reproach, the use of the enthalpy loop would have permitted closer agreement between analysis and experiment. Since the inlet enthalpy and the correlations are both suspect, the enthalpy loop was not included in this procedure.

The liquid run presented herein was analyzed for 18 seconds before a pressure lower than barometric was encountered. At 19 and at 20 seconds, the flow rate was reduced. The adjusted flow rates are shown on the experimental flow-rate schedule of figure 9.

During the transient analysis of this run, equation (3) was used as the heat-transfer correlation in the two-phase region, and equation (B4) was used in the all-gas region. The experimental data from which these equations were developed came closest to the

conditions to be analyzed.

Overall characteristics. - The experimental and predicted exit fluid temperatures are presented as a function of time in figure 15. The calculated values are consistently lower than the experimental values. The curves diverge significantly for the first 6 seconds to a difference of 43° R (23.9° K). At 18 seconds, the difference between predicted and experimental values has increased slowly to 58° R (32.2° K). A first interpretation of this figure might be that the heat-transfer correlations are predicting too little heat transfer to the fluid. The same low exit temperatures, relative to experimental, could also occur if the interpretation of the experimental inlet enthalpy was on the low side. The disparity could therefore result from one or the other of these conditions or from a combination thereof. The same trend would result from time lag in the exit fluid thermocouple, but this possibility is reduced by the close agreement between experiment and

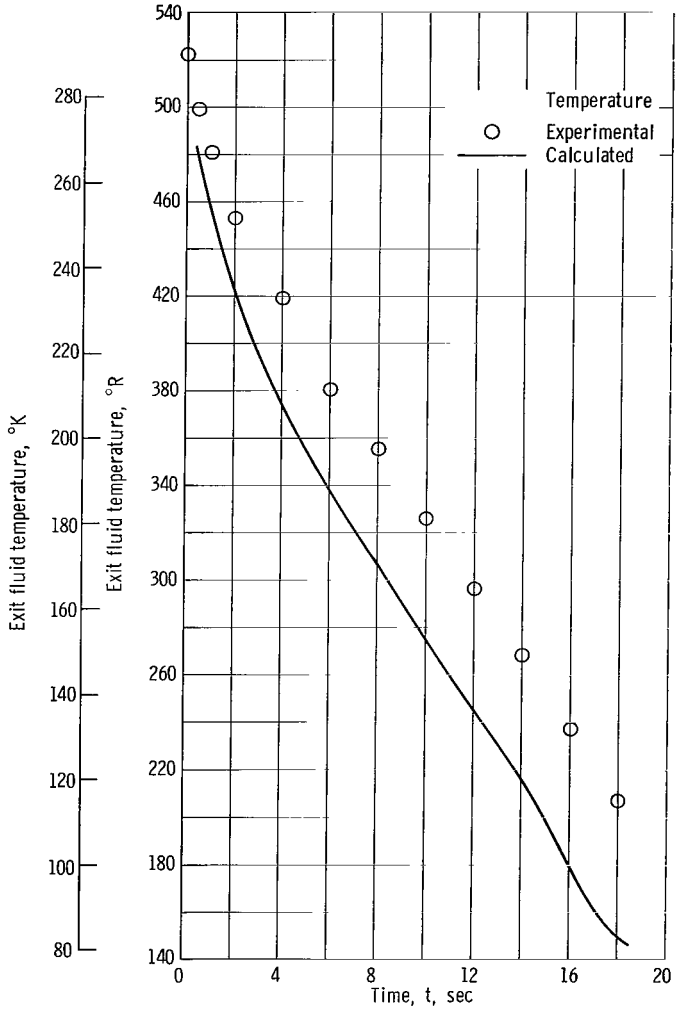

Figure 15. - Comparison of experimental and calculated exit fluid temperatures. Liquid run.

prediction with the gas run.

Figure 16 presents a comparison of the experimental and predicted pressure drop from inlet to exit plenum during the run. The calculated pressure drop is about 46 percent of the experimental at 1.0 second and increases to 90 percent of the experimental value at 18 seconds. At 19 and 20 seconds, it was necessary to reduce the flow rate to avoid pressures below barometric. At these times, the calculated pressure drops were 82 and 88 percent of experimental, respectively, which indicates that for these flow conditions the 2-percent reduction in flow rate results in a significant reduction in overall pressure drop.

Figure 16 verifies the trends indicated in figure 15 due to the relation between pressure drop and heat transfer. The low calculated pressure drop corresponds to the low calculated exit temperature. Both figures indicate that either there is insufficient calculated heat transfer to the fluid or there is an error in the inlet enthalpy of the fluid.

Figure 17 compares the experimental and calculated material temperatures along the length of the test section at 5, 10, and 20 seconds. This figure reflects the predicted and experimental chilldown of the material and permits some enlightening comparisons. If local disparities are ignored, the predicted and experimental material temperatures, on an overall basis, are relatively close as a function of time. This similarity indicates that the material chilldown rate compares well with experiment, while the previous two figures indicated that the fluid was not picking up enough heat. These indications then begin to verify the probability that the disparities in exit fluid temperature and pressure drop are more closely related to errors in inlet enthalpy than to deficient heat-transfer coefficients.

Local characteristics. - The predicted and experimental material temperatures along the length of the test section (fig. 17) provide a good indication of the accuracy of the analytical procedure locally. Before the predicted values are discussed, it should be pointed out that the experimental values are somewhat suspect at the 26.5-, 30.5-, and 52.5-inch (67.3-, 77.5-, and 133.4-cm) stations. During a chilldown run, the liquid penetrates farther into the passage with time. Material temperature patterns generally move down the tube with time. The indicated temperatures at the above mentioned locations are believed to form false stationary peaks. According to the predicted temperatures starting at the inlet and progressing toward the exit, the first 3-inch-long (7.62-cm-long) thin-walled section cools down rapidly. A peak temperature forms at about 5 inches (12.7 cm) followed by a valley which, at 5 seconds, ends near the end of the two-phase region. This peak and valley reflect the effect of the change in wall thickness and the characteristics of equation (3). The rise in predicted wall temperature following the valley is attributed to the step decrease in heat-transfer coefficient at the transition from two-phase to gas or from equation (3) to equation (B4).

In the latter half of the passage, the agreement between predicted and measured wall

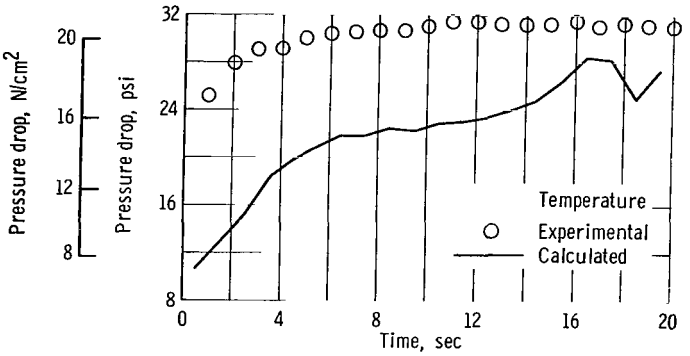

Figure 16. - Comparison of experimental and calculated test-section pressure drop. Liquid run.

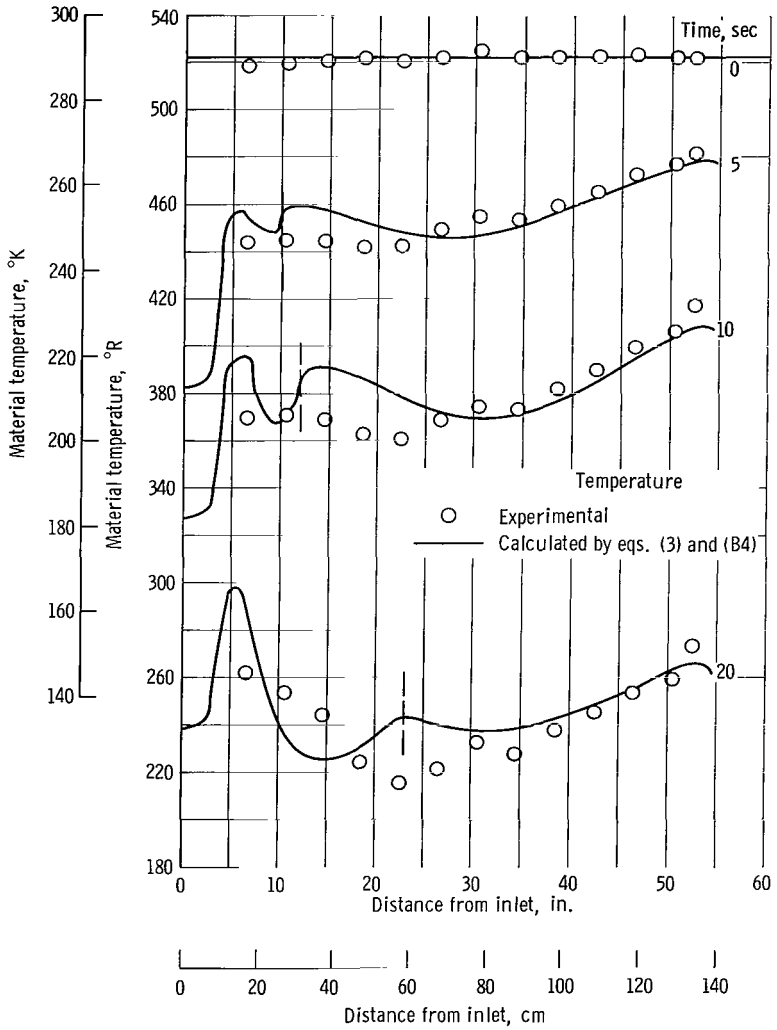

Figure 17. - Comparison of experimental and calculated test-section material temperatures. Liquid run.

temperatures is very good throughout the run. In this region, the fluid temperature is generally above 200° R (111° K).

Figure 18 permits a closer study of the influence of the heat-transfer correlations on the material temperatures. The predicted and experimental material temperature along the length at 5 seconds are presented along with a plot of the heat-transfer coefficients calculated for the 5-second condition. The experimental material temperatures have been smoothed.

Consider first the heat-transfer coefficient. In the two-phase region, the correlation is strongly dependent on quality. The quality is assumed to be zero at the inlet and was calculated to be 1.0 at about 10 inches (25.4 cm). The heat-transfer coefficient increased by a factor of 5.4 from the first 1-inch (2.54-cm) increment to the 10th. Between the 10th and 11th increments, the two-phase region ends, and the gas region begins. The heat-transfer correlation decreases by nearly 28 percent between these increments. In the all-gas region, the heat-transfer coefficient increases fairly smoothly, reflecting the change in gas temperature and the temperature-dependent fluid properties.

The characteristics of the heat-transfer-coefficient curve are reflected in the material-temperature curve. If the test section had been of constant cross section in-

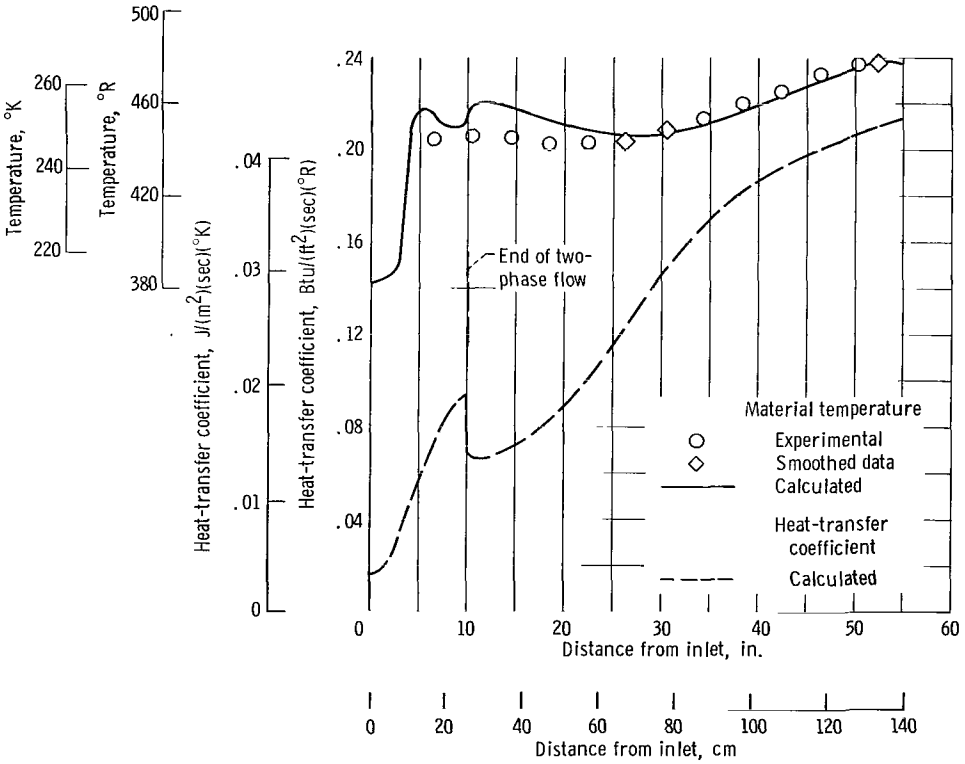

Figure 18. - Comparison of calculated heat-transfer coefficients with material temperatures at 5.0 seconds. Liquid run.

stead of thin-walled tubing for the first 3 inches (7.62 cm), the wall-temperature profile would have been a mirror image of the heat-transfer coefficient. In the gas region, the decreasing temperature difference between wall and fluid reduces the change caused by the increasing heat-transfer coefficient. In the cold-gas region following the end of the two-phase region, the predicted material temperature lags the experimental values. This lag indicates that the gas correlation, when extrapolated into this region, provides lower heat-transfer coefficients than required.

Two significant points are indicated in figures 17 and 18. The first is that the sharp variations in predicted material temperatures are a result of the characteristics of the correlations used. These sharp variations are not verified by experimental temperatures and are indicative of a limitation of the analytical procedure. If the predicted material temperatures are used for stress analysis of reactor members, high thermal stresses will be calculated in the material surrounding the fluid as it makes the transition from two-phase hydrogen to cold gas. The second point is that, considering the chilldown of the entire mass of the test section, the analytical procedure prediction compares well

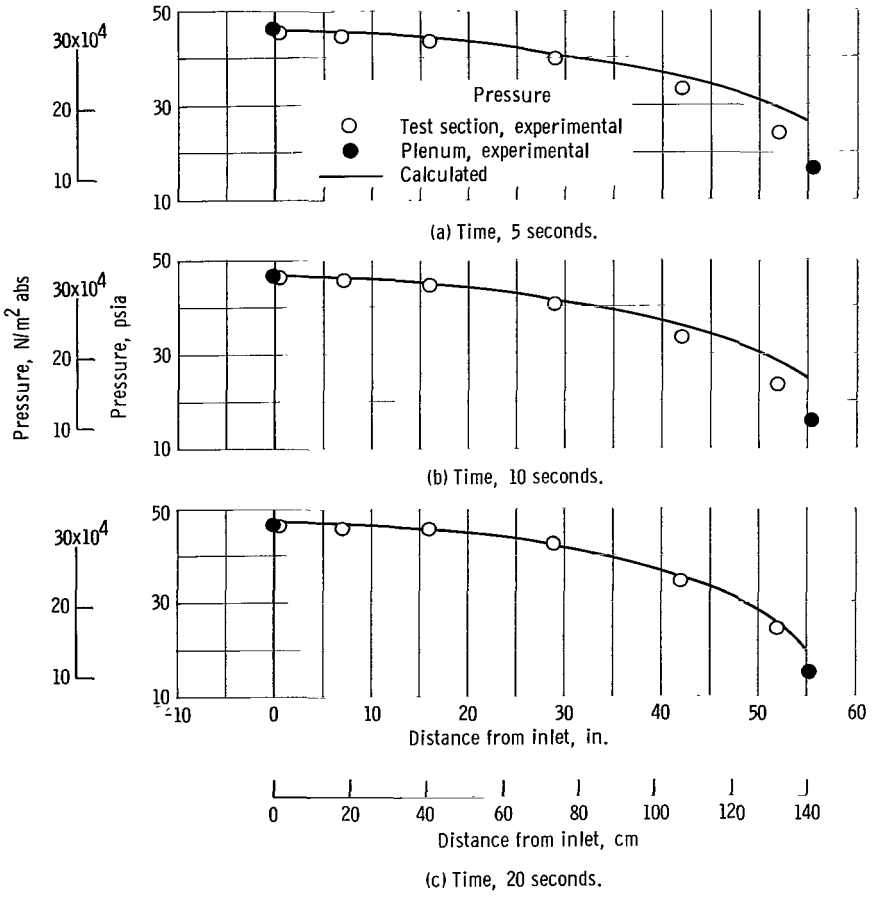

Figure 19. - Comparison of experimental and calculated pressures along length at 5, 10, and 20 seconds. Liquid run.

with experiment. This agreement then is in contradiction to the disparities indicated by fluid temperature rise and fluid pressure drop.

Figure 19 presents a comparison of local experimental and calculated static pressures along the passage at various times during the transient. The experimental plenum pressures are also indicated. Close agreement is maintained between predicted and experimental values until the divergence near the end of the passage. A point made in reference 8 in discussing the pressure loss in a heated passage with liquid entering and gas leaving was that the significant pressure loss occurred in that section of the passage containing all gas. The pressure loss in that portion of the passage containing two-phase hydrogen is relatively small. By this logic, if the assumed inlet enthalpy or quality of the hydrogen is low, the calculated pressure loss will be low because a disproportionate length of the passage will be required to vaporize the liquid. Figures 16 and 19 indicate that this could be the case for this liquid run.

Inlet quality and flow-rate variation effects at 5.0 seconds. - A study was made using the wall-temperature distribution and inlet pressure at 5.0 seconds to evaluate the effects of variations in inlet quality and flow rate on the predicted pressure drop and the total heat added to the tube. The flow rate was varied incrementally ±6.5 percent from the experimental values while the inlet enthalpy of -90.61 Btu per pound (-210 J/g) (saturated liquid) was held constant. This variation more than covers the expected flow measurement error. While holding the flow rate constant, the inlet quality was varied incrementally from a liquid subcooled 5° R (2.78° K) to a quality of 0.31, which represents a range of inlet enthalpy from -110 to -40 Btu per pound (-256 to -93 J/g). Visual assessment of inlet quality could easily span this range. The analytical procedure was used in the same fashion as when performing the parametric studies of reference 8.

The influence of changes in flow rate on the calculated test-section pressure drop and on the heat picked up by the fluid in traversing the passage is shown in figure 20. The vertical dashed line marks the flow rate of 0.00507 pound per second (0.0023 kg/sec) used in the transient analysis at 5 seconds. The pressure drop changes significantly with flow rate. In this case, ±2.0-percent changes in flow rate correspond to +7.1- and -5.6-percent changes in calculated pressure drop. This relation is presented as characteristic of the effect that the rates of change with flow rate are dependent on the wall temperature and other inlet conditions. As was noted previously, the 2-percent reduction in flow rate at 19 and 20 seconds resulted in calculated pressures which were 18 and 12 percent, respectively, below experimental values. The actual pressure drop calculated before the 2-percent flow rate reduction is not retained in the analytical procedure output, but provides an indication of the variation in magnitude of this effect.

The change in total heat transfer from the wall to the fluid is slight with changes in flow rate ($<\pm 0.5$-percent change in heat transfer for a +2.0-percent change in flow rate). This variation indicates that significant changes in assumed flow rate could be made with-

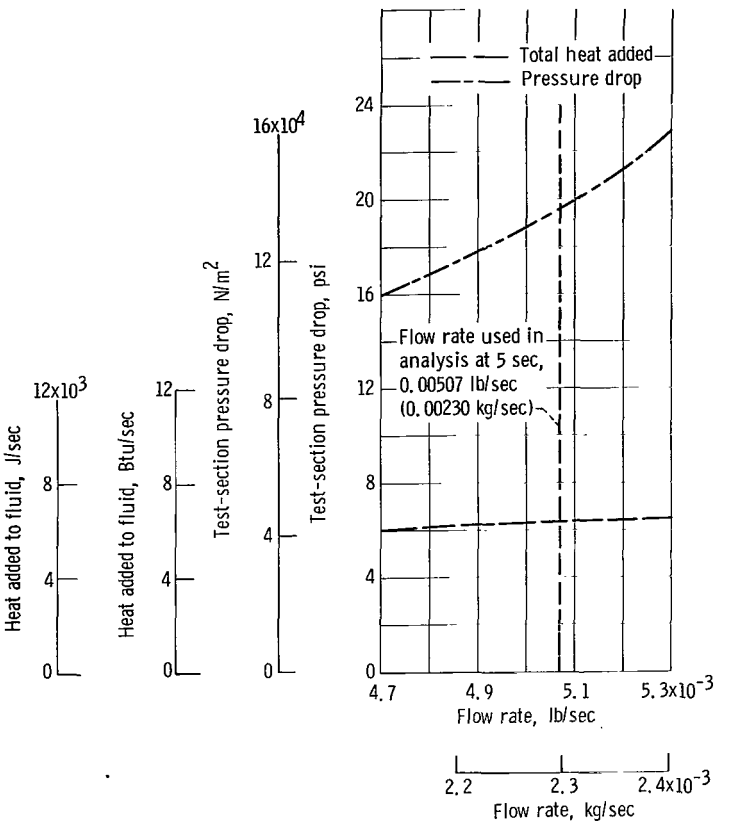

Figure 20. - Effect of flow rate on calculated test-section pressure drop and heat added to fluid. Liquid run; 5-second conditions.

out a significant effect on the chilldown rate of the test section. The experimental pressure drop at 6 seconds was 30 psi (2.07×10^5 N/m^2). Matching this value with a calculated value would require an increase in flow rate of approximately 7.5 percent. Because the estimated accuracy of the experimental flow rate is ±2.0 percent, it is unlikely that the disparity between predicted and experimental values can be attributed to flow rate alone.

The influence of inlet enthalpy on calculated pressure drop, exit fluid temperature, and heat added to the fluid is presented in figure 21. The vertical dashed line marks the enthalpy for a saturated liquid that was assumed for transient analysis at 5 seconds. Inlet enthalpy values to the left of this line represent subcooled liquid and to the right represent two-phase hydrogen. Negative pressures were calculated with an inlet quality of -40 Btu per pound (-93 J/g); therefore, only the range from -110 to -50 Btu per pound (-256 to -116 J/g) is presented.

The pressure drop is strongly influenced by the change in inlet enthalpy. Over the range of inlet enthalpy presented, the pressure drop varies from -20 to +45 percent of

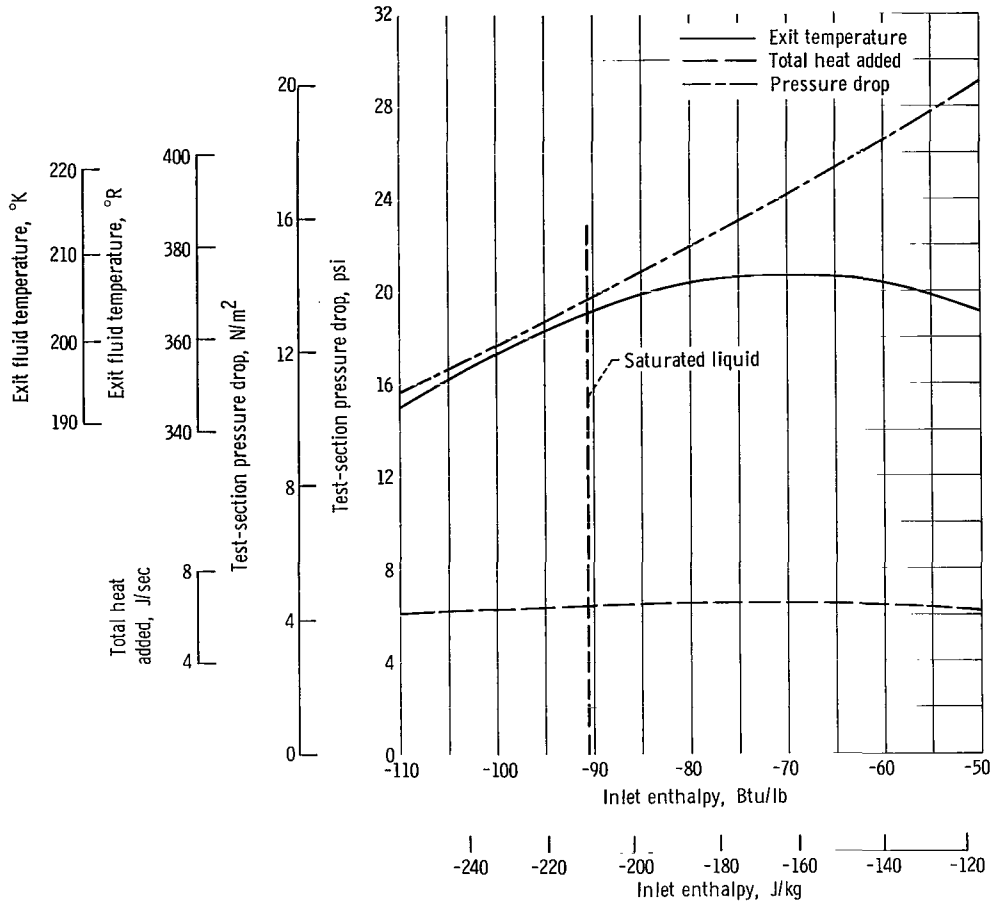

Figure 21. - Effect of inlet enthalpy on calculated pressure drop, exit fluid temperature, and heat added to fluid.

the pressure drop calculated for the saturated-liquid inlet condition. This error would be largest at the beginning of the run, when the fluid is being evaporated by heat addition from the inlet plenum. In this period also, the largest discrepancies between calculated and experimental pressure drops occur. Although the pressure drop is continually increasing, the exit fluid temperature reaches a maximum and then decreases as the inlet enthalpy is increased. This phenomenon occurs as the temperature difference between wall and fluid decreases faster than the heat-transfer coefficient increases; thus, the product decreases. This characteristic is reflected also in the heat-added curve.

The curves indicating the heat transfer from wall to fluid are again flat and nearly independent of changes in inlet quality. Thus, it is evident that the rate of material chilldown is relatively independent of the accuracy of the inlet quality or flow rate and that the close agreement indicated by figure 17 was to be expected.

The disparities between experimental and calculated pressure drop (fig. 16) and exit fluid temperature (fig. 15) can be attributed partly to possible inaccuracies in inter-

pretation of the experimental values for inlet quality and flow rate. It is apparent that a combination of an increase in flow rate and an increase in inlet enthalpy would permit convergence on the experimental pressure drop without excessive changes in the parameters and with an insignificant change in the overall heat-transfer rate.

The strong influence of inlet quality or enthalpy on the calculated pressure drop in a single passage is a significant indication of its probable effect on reactor components containing parallel passages. If, in the real case, the parallel passages do not receive fluid of uniform inlet quality, velocity, pressure, etc., poor agreement between predicted and experimental results will be obtained. The experimental results will reflect the inlet quality maldistribution characteristics indicated by figure 21. The flow rate in each passage will adjust itself according to the inlet quality so that all passages have the same pressure drop. A transient analysis performed assuming the same total flow rate and uniform passage inlet conditions will predict different overall pressure drop, flow distribution, and radial temperature profiles. An example of the variation in flow distribution between two parallel passages, with changes in the inlet enthalpy to the individual passages, is presented in reference 8.

This potential source of disparity between predicted and experimental results is presented to emphasize the need for careful design of the channels supplying parallel passages to avoid maldistribution if useful analysis and simulation of the system component is desired. An alternative solution would be the generation of an inlet distribution function for the parallel passages for use in analysis.

SUMMARY OF RESULTS

A procedure developed for flow and heat-transfer analysis during the startup transient of nuclear-rocket components was applied to a thick-walled aluminum test section. A series of chilldown experiments was performed, to evaluate the analytical procedure. The following results were obtained.

Gas Run

1. Predicted material temperatures were within 10° R (5.56° K) of the experimental values along the length of the tube.

2. The calculated heat given by the tube was about 5 percent less than indicated by experiment.

3. The pressure drops predicted by using the analytical procedure were approximately 3 percent lower than those obtained experimentally.

4. In the extrapolated region, where the inlet enthalpy was linearly decreased to saturated gas, equations (B2), (B3), and (B4) appear to be equally applicable.

5. Results obtained using equation (B5) begin to change relative to the results of the other equations after the inlet fluid temperature drops below 250° R (139° K). The shift is gradual, however, and is only beginning to become significant when the average fluid temperature in the passage is below 225° R (125° K).

Liquid Run

1. Experimentally, there was no way to measure the enthalpy of hydrogen entering the test section if it were in the two-phase region. The pressure and temperature measurements are sufficient to define enthalpy only in a subcooled liquid or a superheated gas. Various efforts, including refined experimental techniques, mechanical separation of phases, and visual observation, were made to reduce inaccuracy caused by the lack of a direct enthalpy measurement.

2. The heat-transfer correlations, as applied, result in the prediction of distorted wall-temperature profiles, which are not verified by experimental measurements. The distortions occur in the high-quality two-phase region and continue into the cold-gas region. Careful heat-transfer research is required in this flow region to provide correlations which correct the distortions.

3. On an overall basis, considering mass averaged temperatures of the test section, the agreement between experimental and predicted chilldown is good. This agreement also was relatively independent of the accuracy of inlet condition and flow rate.

4. Predicted pressure drop and exit temperatures compared poorly with experimental values. Pressure drop values were calculated which varied from unrealistically high values to values less than 50 percent of experimental. Calculated exit fluid temperatures were consistently lower than experimental values.

5. The predicted pressure drop was sensitive to slight changes in inlet quality and flow rate. Much of the deviation between predicted and experimental pressure and fluid temperature results could be removed by adjustment of inlet quality and flow rate within the range of their experimental accuracies.

Lewis Research Center,
National Aeronautics and Space Administration,
Cleveland, Ohio, July 12, 1967,
122-29-01-33-22.

APPENDIX A

SYMBOLS

A	area, ft^2; m^2
a	exponent of Reynolds number in heat-transfer correlation (eq. (B1))
b	exponent of Prandtl number in heat-transfer correlation (eq. (B1))
Bo	boiling number, $Q/G\lambda A_s$
C	exponent of wall-to-bulk temperature ratio in eq. (B4)
c	coefficient in heat-transfer correlation (eq. (B1))
C_p	specific heat at constant pressure, Btu/(lb mass)(^oR); J/(kg)(^oK)
D	hydraulic diameter, ft; m
f	Fanning friction factor
G	mass flow rate per unit area, lb mass/(sec)(ft^2); kg/(sec)(m^2)
g	gravitational constant, 32.174 (lb mass)(ft)/(lb force)(sec^2); 32.174 (kg)(m)/(N)(sec^2)
H	enthalpy, Btu/lb mass; J/g
h	heat-transfer coefficient, Btu/(sec)(ft^2)(^oR); J/Btu; 778 (m)(N)/J
J	Joule constant, 778 (ft)(lb force)/Btu; (m)(N)/J
j	point between increments (exit to increment M, inlet to increment M + 1), see fig. 5(a)
K	loss coefficient for restriction, determined experimentally
K'	entrance pressure loss coefficient
K''	exit loss coefficient
k	thermal conductivity, Btu/(sec)(ft)(^oR); J/(sec)(m)(^oK)
L	length from entrance of tube to center of increment, ft; cm
ℓ	length of increment, ft; m
M	index for longitudinal increments
Nu	Nusselt number, hD/k
n	exponent of temperature ratio in heat-transfer correlation (eq. (B1))
P	pressure, lb force/$in.^2$; N/cm^2

Pr	Prandtl number, $C_p\mu/k$
Q	heat flow per increment, Btu/sec; J/sec
Re	Reynolds number, GD/μ
T	temperature, ^oR; ^oK
t	time, sec
V	velocity, ft/sec; m/sec
$\dot{w}$	mass flow rate, lb mass/sec; kg/sec
X_{tt}	Martinelli parameter
x	quality, mass fraction of vapor
α	proportionality constant for eq. (B5) (k in ref. 9), $Btu/(^oR)(lb\ mass^{0.8})(hr^{0.2})(ft^{0.2})$; $J/(^oK)(kg^{0.8})(hr^{0.2})(m^{0.2})$
λ	heat of vaporization, Btu/lb mass
μ	viscosity, lb mass/(ft)(sec); kg/(m)(sec)
ρ	density, lb mass/ft^3; kg/m^3

Subscripts:

atm	atmospheric conditions
av	average cross increment
b	bulk
f	film
fm	film mean
fr	friction
g	saturated gas
i	initial conditions
in	inlet plenum
j	point between increments (exit to increment M, inlet to increment M + 1), see fig. 5(a)
l	saturated liquid
M	increment
mom	momentum
n	exit of last increment

out	exit plenum
res	restriction
s	surface
st	static
tot	total across test section
tp	two phase
w	wall

APPENDIX B

STATUS OF CORRELATIONS

Forced-Convection Gas Heat Transfer

Heat transfer to gases, including hydrogen, has been the subject of many investigations. Some excellent discussions of correlations for gas heat transfer are available in the literature such as references 10 to 13. In each case, the discussion leads to a recommended correlation for a specific range of conditions. The discussion which follows includes the uniqueness of the conditions to be analyzed during nuclear-rocket startup as compared with the conditions under which various heat-transfer experiments have been performed.

The experimental results of collective and individual gas heat-transfer studies have been correlated by several methods. Typical of the methods is an empirical equation containing dimensionless groupings of the following form:

$$Nu = cRe^{a}Pr^{b}\left(\frac{T_w}{T_b}\right)^{n} \tag{B1}$$

The constant c and the exponents a, b, and n are determined empirically. The values most often encountered for a and b are 0.8 and 0.4, respectively.

The physical properties involved in the dimensionless groups (Nu, Re, and Pr) have been evaluated at various reference temperatures; bulk, film, and wall temperatures are typical. Correlations based on bulk or wall temperature may generally be applied more directly in solving heat-transfer problems. Classically, the preference is for evaluating the transport properties of the fluid at an intermediate or film temperature, especially when considering high values of T_w/T_b. As discussed in reference 12 for nearly perfect gases and fully developed flow, it has been demonstrated that equally satisfactory correlations can be obtained by evaluating the fluid properties at bulk, film, or wall temperatures if suitable coefficients and exponents for the dimensionless parameters are used. The T_w/T_b term raised to the n power is sometimes considered as a term modifying a bulk Reynolds number to film conditions.

The foregoing discussion infers that the most convenient form of a correlation could be used to perform a reasonably accurate heat-transfer analysis. Unfortunately, this inference is not entirely true. The experiments on which the correlations are based cover a limited range of conditions relative to those occurring during the bootstrap startup of a nuclear rocket. More specifically, in a nuclear rocket, heat transfer to the

gas must be evaluated under these conditions:

(1) The temperature and velocity profiles develop concurrently

(2) The bulk temperatures are low following the transition from two-phase to all-gas flow

(3) Parahydrogen rather than normal hydrogen is the working fluid

A review of the heat-transfer experiments reported in the literature reveals that at subcritical pressures in all cases an unheated length preceded the heated section, that the lowest bulk temperatures encountered were 135° R (75° K), and that the experiments were performed with normal hydrogen.

In general, the heat-transfer coefficient is enhanced by entrance effects (ref. 14). In reference 12, the anomaly of a decrease in heat transfer with increase in temperature difference (higher T_w/T_b) is discussed. Unpublished experimental studies of H. J. Gladden of Lewis indicate a decrease in heat transfer with decrease in bulk temperature below 300° R (167° K) at a constant L/D. The changes in the fluid property group $k^{0.6}C_p^{0.4}/\mu^{0.4}$ with temperature for both normal and parahydrogen are shown in reference 9.

Further research and analysis is required before existing correlations can be extended into some regions of gas heat transfer in a nuclear rocket. In the absence of proven correlations relating the variables L/D, T_w/T_b, and fluid properties over the required range, it was necessary to use existing correlations and extrapolate them so that the transient analysis could be performed.

Four correlations were selected from the literature and included in the FLØW analysis procedure; they were selected by an input call number. The results of applying them to transient analysis are presented in the RESULTS AND DISCUSSION section of this report. The correlations are described briefly in the following paragraphs.

Kays and London (ref. 4) recommend the following correlation for heat transfer to gas flowing in long circular ducts:

$$Nu_b = 0.021\, Re_b^{0.8} Pr_b^{0.33} \left(\frac{T_w}{T_b}\right)^{-0.575} \tag{B2}$$

This correlation has had wide use in heat-exchanger design and is of the form indicated by equation (B1).

A literature survey by Thomas (ref. 15) directed toward recommending a correlation for gas-heat-transfer analysis in a nuclear rocket resulted in

$$Nu_b = 0.025\, Re_b^{0.8} Pr_b^{0.4} \left(\frac{T_w}{T_b}\right)^{-0.55} \left[1 + 0.3\left(\frac{D}{L}\right)^{0.7}\right] \tag{B3}$$

This correlation contains a term which enhances the heat transfer near the entrance.

Miller and Taylor (ref. 11) presented a correlation for high surface-to-bulk temperature ratios:

$$Nu_b = 0.021\, Re_b^{0.8} Pr_b^{0.4} \left(\frac{T_w}{T_b}\right)^{-C} \tag{B4}$$

where

$$C = 0.29 + 0.0019\,\frac{L}{D}$$

The supporting experiments for their correlation came the closest to the conditions to be analyzed during the startup.

Simoneau and Hendricks (ref. 9) presented a simplified correlation wherein the fluid property group $k^{0.6} C_p^{0.4}/\mu^{0.4}$ is evaluated at one temperature and included in the constant α, resulting in an equation of the form

$$h = \alpha (\rho V)_b^{0.8} D^{-0.2} \left(\frac{T_b}{T_w}\right)^{0.5} \tag{B5}$$

where α (k in ref. 9) is a constant for any given gas. For hydrogen $\alpha = 0.048$. This correlation is not recommended for bulk temperatures near or below critical. It was included for comparison with the other correlations to illustrate the effect of neglecting the change in fluid properties with temperature.

Two-Phase Film Boiling in Hydrogen

Various pool boiling experiments for hydrogen have placed the temperature difference between wall and fluid for the end of nucleate boiling in the range 2° to 20° R (1.11° to 11.1° K). Since this low temperature difference is not expected to prevail during a bootstrap operation, only film boiling was considered.

Hendricks and co-workers (ref. 5) have investigated the forced convection film-boiling region at subcritical pressures. With a liquid core and a gas annulus as a flow model and the Martinelli parameter as a variable, the following correlation was obtained:

$$Nu_f = \frac{0.023\ Re_{tp}^{0.8} Pr_f^{0.4}}{0.611 + 1.93\ X_{tt}}$$

This equation is presented and the various terms are defined in the section ANALYTICAL PROCEDURE.

The following experimental conditions were considered in presenting this correlation:

Pressure, psia; N/m^2	30 to 70; 2.06×10^5 to 4.82×10^5
Heat flux, Btu/(in.^{2})(sec); J/(cm^2)(sec)	to 1.0; to 163.4
Wall-to-bulk temperature difference, ^oR; ^oK	50 to 750; 27.8 to 417
Inlet quality	subcooled to 0.8
Outside diameter, in.; cm	0.375; 0.952
Wall thickness, in.; cm	0.031; 0.079
Heated length, in.; cm	12; 30.5

In applying this correlation to a nuclear-rocket startup there are two limitations:

(1) An unheated length preceded the heated length; thus, no information was available on the influence of abrupt contractions on film-boiling heat transfer.

(2) The data did not extend to a quality of 1.0.

As is developed in the section RESULTS AND DISCUSSION the predicted transition from two phases to gas is debatable, and further research is required to determine whether the two-phase correlation or the gas correlation, or both, contain the discrepancies.

Another correlation was found to cluster experimental data better than equation (3), it is presented in reference 16 and is identical to equation (3) except for the inclusion of a boiling number Bo. A transient analysis, not included in this report, was performed with that correlation, and the heat-transfer coefficients defined were essentially identical to those determined by equation (3). Various other correlations have been proposed and are analyzed and reviewed in reference 17.

Pressure Drop

The pressure drop in a passage may be considered as consisting of four parts: (1) entrance losses, (2) friction and momentum losses, (3) losses due to restrictions, and (4) exit losses. The entrance losses, losses due to restrictions, and exit losses are calculated from equations (1), (10), and (13), respectively, by the proper selection of the respective loss coefficients.

In a length increment free of restrictions, the pressure drop is the summation of

momentum and friction losses:

$$\Delta P = \Delta P_{fr} + \Delta P_{mom} \tag{B6}$$

The momentum pressure drop is calculated from equation (9). In the two-phase film-boiling region, this term is usually dominant. The Martinelli parameter which was developed with two-phase two-component (water and air, oil and air) isothermal flow was considered in formulating the analysis. Its contribution to pressure drop was negligible relative to the momentum losses occurring with film boiling.

Many investigators have studied the problems of determining accurate friction factors. In single-phase, isothermal, incompressible, turbulent flow the Fanning friction factor for smooth pipes is well correlated by the von Karman-Nikuradse equation as presented in reference 18.

$$\frac{1}{\sqrt{f}} = 4.0 \log\left(Re\sqrt{f}\right) - 0.4 \tag{B7}$$

Several relations for friction factor have been developed for limited ranges (ref. 18), such as the Koo equation

$$f = 0.0014 + \frac{0.125}{(Re_b)^{0.32}} \tag{B8}$$

which is valid for Reynolds numbers ranging from 3000 to 300 000. Based on experimental data, the following equation is valid for bulk Reynolds numbers from 5000 to 200 000:

$$f = \frac{0.046}{(Re_b)^{0.2}} \tag{B9}$$

The previously mentioned friction factors are based on isothermal flow. Humble, Lowdermilk, and Desmom measured and reported (ref. 6) friction factors for air flow with heat transfer for values of T_w/T_b as high as 2.5. As T_w/T_b increased, the values of f fell progressively lower than conventional values of f without heat transfer. The data considered could be correlated by the equation

$$f = \frac{T_b}{T_f \left[4.0 \log \left(Re_f \frac{\rho_f}{\rho_b} \sqrt{f \frac{T_b}{T_f}} \right) - 0.4 \right]^2} \tag{B10}$$

where

$$Re_f = \frac{GD}{\mu_f}$$

The preceding equation was considered applicable to the conditions analyzed in the passage.

APPENDIX C

LIQUID-HYDROGEN CHILLDOWN RUN EXPERIMENTAL DATA

Inlet conditions as a function of time for two additional chilldown tests (runs 53 and 55) are presented in figures 22 and 23. Experimental material temperatures, fluid pressures, and exit fluid temperatures in the test section are presented according to location at selected times in tables II and III.

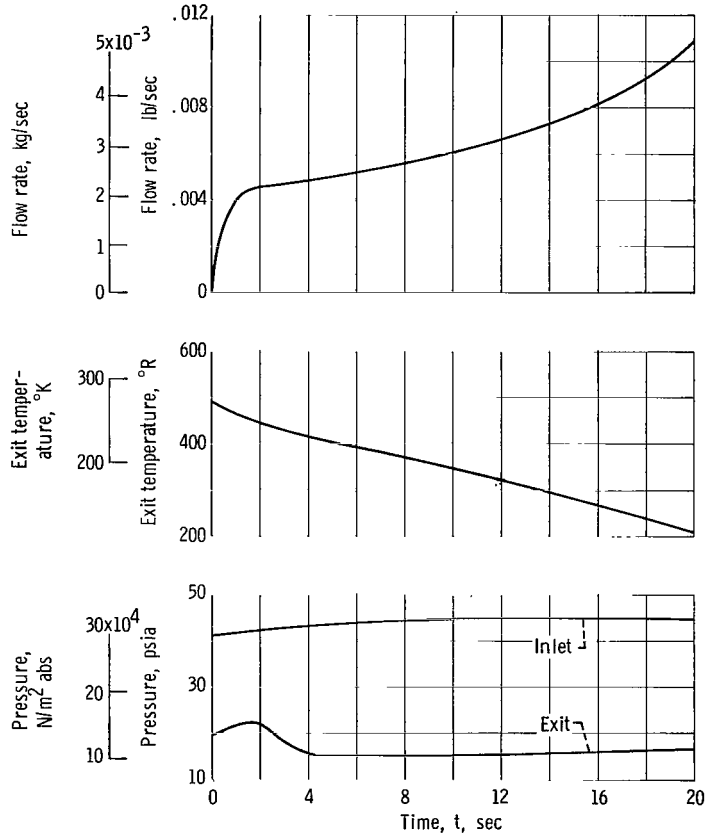

Figure 22. - Flow conditions for run 53.

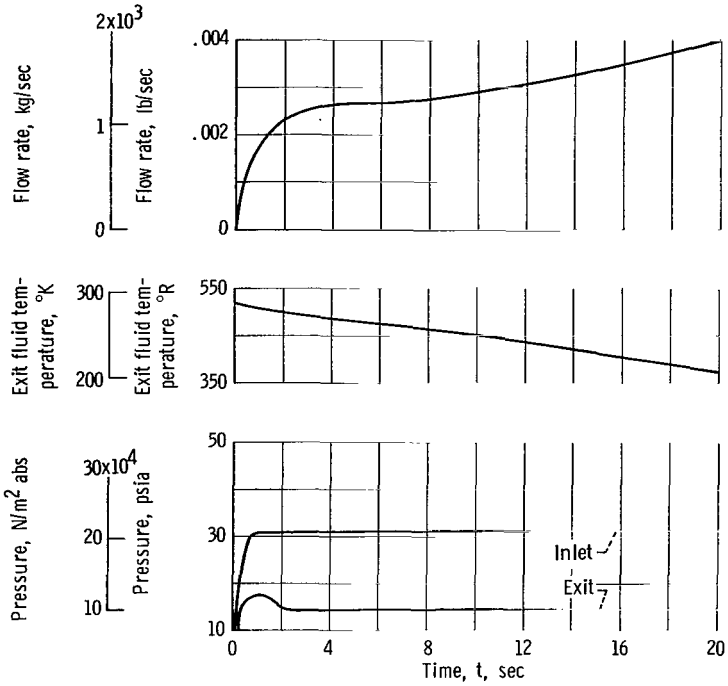

Figure 23. - Flow conditions for run 55.

TABLE II. - EXPERIMENTAL MATERIAL TEMPERATURES

AND FLUID PRESSURES FOR RUN 53

(a) U. S. Customary Units

Length from entrance of tube to center of increment, L, in.	Time, sec						
	0	1	2	5	10	15	20
	Material temperature, ^{o}R						
6.5	451.1	447.3	435.3	396.4	335.4	283.7	240.8
10.5	461.5	458.1	444.3	403.5	339.8	284.5	234.09
14.5	470.5	467.8	454.5	411.9	343.0	284.4	229.3
18.5	477.1	474.9	459.9	414.4	340.7	276.0	213.6
22.5	481.9	479.9	465.3	418.7	343.2	274.3	205.0
26.5	487.2	485.8	472.8	427.9	351.6	282.6	205.6
30.5	492.2	490.6	477.4	433.5	357.0	288.1	207.6
34.5	493.8	492.6	479.7	435.7	358.0	288.0	206.6
38.5	495.0	494.4	483.1	442.2	366.3	295.4	217.5
42.5	497.5	496.8	486.7	447.6	373.9	304.0	229.5
46.5	499.7	499.2	490.8	455.1	382.5	310.9	235.7
50.5	499.6	499.3	491.8	459.5	389.7	318.1	241.2
52.5	499.2	499.0	492.5	463.6	398.1	328.6	255.0
	Static pressure, psia						
7.0	-----	29.7	41.4	43.3	44.9	45.5	45.6
16.0	-----	28.7	39.6	41.6	43.2	44.0	44.2
29.0	-----	26.7	36.4	38.3	40.5	42.3	43.6
42.0	-----	23.9	31.0	31.6	33.4	34.7	36.0
52.0	-----	21.8	24.9	22.6	23.8	24.6	25.8

TABLE II. - Concluded. EXPERIMENTAL MATERIAL TEMPERATURES AND FLUID PRESSURES FOR RUN 53

(b) SI Units

Length from entrance of tube to center of increment, L, cm	Time, sec						
	0	1	2	5	10	15	20
	Material temperature, ^{o}K						
16.51	250.6	248.5	241.8	220.2	186.3	157.6	133.8
26.67	256.4	254.5	246.8	224.2	188.8	158.1	130.5
36.83	261.4	259.9	252.5	228.8	190.6	158.0	127.4
46.99	265.1	263.8	255.5	230.2	189.3	153.3	118.7
57.15	267.7	266.6	258.5	232.6	190.7	152.4	113.9
67.31	270.7	269.9	262.7	237.7	195.3	156.9	114.2
77.47	273.4	272.6	265.2	240.8	198.3	160.1	115.3
87.63	274.3	273.7	266.5	242.1	198.9	160.0	114.8
97.79	275	274.7	268.4	245.7	203.5	164.1	120.8
107.95	276.4	276.0	270.4	248.7	207.7	168.9	127.5
118.11	277.6	277.3	272.7	252.8	212.5	172.7	130.9
128.27	277.6	277.4	273.2	255.3	216.5	176.7	134
133.35	277.3	277.2	273.6	257.6	221.2	182.6	141.7
	Static pressure, N/m^2						
17.78×10^5	-----	2.05×10^5	2.85×10^5	2.99×10^5	3.10×10^5	3.14×10^5	3.14×10^5
40.6	-----	1.98	2.73	2.87	2.98	3.03	3.05
73.66	-----	1.84	2.51	2.64	2.79	2.92	3.01
106.68	-----	1.65	2.14	2.18	2.30	2.39	2.48
132.08	-----	1.50	1.72	1.56	1.64	1.70	1.78

TABLE III. - EXPERIMENTAL MATERIAL TEMPERATURES

AND FLUID PRESSURES FOR RUN 55

(a) U. S. Customary Units

Length from entrance of tube to center of increment, L, in.	Time, sec						
	0	1	2	5	10	15	20
	Material temperature, ^{o}R						
6.5	513.2	505.6	493.5	456.5	398.7	350.4	311.3
10.5	513.8	507.0	495.7	462.1	403.3	351.1	308.6
14.5	514.9	509.7	498.2	465.4	408.3	354.8	309.1
18.5	516.4	510.7	499.1	465.5	401.6	355.0	305.9
22.5	515.3	510.3	499.1	466.4	410.1	357.6	307.6
26.5	516.3	512.3	502.3	471.4	417.6	365.8	316.1
30.5	518.4	514.7	505.4	476.3	424.1	372.7	325.2
34.5	516.8	513.7	504.9	477.0	425.5	374.4	326.1
38.5	516.0	513.4	506.5	482.3	434.1	384.5	336.2
42.5	516.5	514.5	508.7	487.2	443.0	395.3	347.5
46.5	518.4	517.4	512.3	494.1	453.7	407.1	359.5
50.5	516.9	515.5	511.6	495.8	459.7	416.2	368.2
52.5	515.9	515.0	511.9	497.9	465.8	425.3	380.1
	Static pressure, psia						
7.0	-----	29.5	29.5	29.6	30.4	30.9	30.7
16.0	-----	28.3	28.3	28.4	29.3	30.0	29.9
29.0	-----	23.1	22.8	22.9	24.0	24.9	24.9
42.0	-----	22.3	21.9	21.6	22.5	23.1	23.2
52.0	-----	18.7	17.4	16.4	16.9	17.3	17.3

TABLE III. - Concluded. EXPERIMENTAL MATERIAL TEMPERATURES AND FLUID PRESSURES FOR RUN 55

(b) SI Units

Length from entrance of tube to center of increment, L, cm	Time, sec						
	0	1	2	5	10	15	20
	Material temperature, ^{o}K						
16.51	285.1	280.9	274.1	253.5	221.5	194.7	172.9
26.67	285.4	281.6	275.4	256.7	224.0	195.0	171.4
36.83	286.0	283.1	276.8	258.5	226.8	197.1	171.7
46.99	286.9	283.7	277.3	258.6	227.0	197.2	170.0
57.15	286.2	283.5	277.3	259.1	277.8	198.6	170.9
67.31	286.8	284.6	279.0	261.9	232.0	203.2	175.6
77.47	288	285.9	280.7	264.6	235.6	207.0	180.6
87.63	287.1	285.4	280.5	265.0	236.4	208	181.1
97.79	286.6	285.2	281.3	267.9	241.0	213.6	186.8
108.95	286.9	285.8	282.6	270.6	246.1	219.5	193.0
118.11	288.0	287.4	284.6	274.5	252.0	226.1	199.7
128.27	287.1	286.4	284.2	275.4	255.4	231.2	204.5
133.35	286.5	286.1	284.4	276.6	258.8	236.2	211.1
	Static pressure, N/m^2						
17.78×10^5	-----	2.03×10^5	2.03×10^5	2.04×10^5	2.10×10^5	2.13×10^5	2.12×10^5
40.6	-----	1.95	1.95	1.96	2.02	2.07	2.06
23.66	-----	1.59	1.57	1.58	1.65	1.72	1.72
106.68	-----	1.54	1.51	1.49	1.55	1.59	1.60
132.08	-----	1.29	1.20	1.13	1.17	1.19	1.19

REFERENCES

1. Chenoweth, Francis C.; Pleban, Eugene J.; Clark, John S.; and Sprague, Earl L.: Startup Heat-Transfer and Fluid-Flow Characteristics in a Nuclear-Rocket Reflector. NASA Technical Memorandum, estimated publication date, Oct. 1967.

2. Bagwell, David: TØSS - An IBM-7090 Code for Computing Transient or Steady State Temperature Distributions. Rep. No. K-1494, Oak Ridge Gaseous Diffusion Plant, Dec. 1, 1961.

3. Harry, David P., III: Formulation and Digital Coding of Approximate Hydrogen Properties for Application to Heat-Transfer and Fluid-Flow Computations. NASA TN D-1664, 1963.

4. Kays, W. M.; and London, A. L.: Compact Heat Exchangers. McGraw-Hill Book Co., Inc., 1955.

5. Hendricks, R. C.; Graham, R. W.; Hsu, Y. Y.; and Friedman, R.: Experimental Heat Transfer and Pressure Drop of Liquid Hydrogen Flowing Through a Heated Tube. NASA TN D-765, 1961.

6. Humble, Leroy V.; Lowdermilk, Warren H.; and Desmom, Leland G.: Measurements of Average Heat-Transfer and Friction Coefficients for Subsonic Flow of Air in Smooth Tubes at High Surface and Fluid Temperatures. NACA TR 1020, 1951.

7. Staff of Eng. Div.: Flow of Fluids through Valves, Fittings and Pipe. Tech. Paper No. 410, Crane Co., Chicago, Ill.

8. Watt, James J.: Analysis of Hydrogen Flow Characteristics at Subcritical Pressures. Nuclear Rocket Technology Conference. NASA SP-123, 1966, pp. 118-127.

9. Simoneau, J. R.; and Hendricks, R. C.: A Simple Equation for Correlating Turbulent Heat Transfer to a Gas. Paper presented at the AIChE-ASME Heat Transfer Conference and Products Show, Cleveland, Aug. 9-12, 1964.

10. Clark, John S.: Analytical and Experimental Study of Startup Characteristics of a Full-Scale Unfueled Nuclear-Rocket-Core Assembly. NASA TM X-1231, 1966.

11. Miller, John V.; and Taylor, Maynard F.: Improved Method of Predicting Surface Temperatures in Hydrogen-Cooled Nuclear Rocket Reactor at High Surface-to-Bulk Temperature Ratios. NASA TN D-2594, 1965.

12. Anon.: Review of NERVA Heat Transfer Analysis. Rep. No. RN-S-0092, Aerojet General Corp., 1964.

13. McCarthy, J. R.; and Wolf, H.: Forced Convection Heat Transfer to Gaseous Hydrogen at High Heat Flux and High Pressure in a Smooth, Round, Electrically Heated Tube. ARS J., vol. 30, no. 4, Apr. 1960, pp. 423-425.

14. Eckert, E. R. G.; and Drake, Robert M.: Heat and Mass Transfer. Second ed., McGraw-Hill Book Co., Inc., 1959.

15. Thomas, G. R.: An Interim Study of Single Phase Heat Transfer Correlations Using Hydrogen. Rep. No. WANL-TNR-056, Westinghouse Electrical Corp., 1962.

16. Ellerbrock, Herman H.; Livingood, John N. B.; and Straight, David M.: Fluid-Flow and Heat-Transfer in Nuclear Rockets. Proceedings of the NASA-University Conference on the Science and Technology of Space Exploration. NASA SP-11, vol. 2, 1962, pp. 87-116.

17. Brentari, E. G.; Giarratano, P. J.; and Smith, R. V.: Boiling Heat Transfer for Oxygen, Nitrogen, Hydrogen, and Helium. Tech. Note 317 (NASA CR-68614), National Bureau of Standards, Sept. 20, 1965.

18. McAdams, William H.: Heat Transmission. Third ed., McGraw-Hill Book Co., Inc., 1954.

NASA-Langley, 1967 —— 33 E-3737